

The SAURON project XVI: On the Sources of Ionisation for the Gas in Elliptical and Lenticular Galaxies

Marc Sarzi,^{1*} Joseph C. Shields,² Kevin Schawinski,³ Hyunjin Jeong,⁴ Kristen Shapiro,⁵ Roland Bacon,⁶ Martin Bureau,⁷ Michele Cappellari,⁷ Roger L. Davies,⁷ P. Tim de Zeeuw,^{8,9} Eric Emsellem,⁸, Jesús Falcón-Barroso,¹⁰ Davor Krajnović,⁷ Harald Kuntschner,⁸ Richard M. McDermid,¹¹ Reynier F. Peletier¹² Remco C. E. van den Bosch,¹³ Glen van den Ven,¹⁴ Sukyoung K. Yi,⁴

¹Centre for Astrophysics Research, University of Hertfordshire, College Lane, Hatfield, Herts, AL10 9AB, UK

²Physics & Astronomy Department, Ohio University, Athens, OH 45701 USA

³Yale Center for Astronomy and Astrophysics, Yale University, P.O. Box 208121, New Haven, CT06520, USA

⁴Department of Astronomy, Yonsei University, Seoul 120-749, Korea

⁵UC Berkeley Department of Astronomy, Berkeley, CA 94720, USA

⁶Centre de Recherche Astronomique de Lyon, 9 Avenue Charles André, 69230 Saint Genis Laval, France

⁷Denys Wilkinson Building, University of Oxford, Keble Road, Oxford, United Kingdom

⁸European Southern Observatory, Karl-Schwarzschild-Str 2, 85748 Garching, Germany

⁹Sterrewacht Leiden, Universiteit Leiden, Postbus 9513, 2300 RA Leiden, The Netherlands

¹⁰Instituto de Astrofísica de Canarias, Canarias, Via Lactea s/n, 38700 La Laguna, Tenerife, Spain

¹¹Gemini Observatory, Northern Operations Center, 670 N. Aohoku Place, Hilo, HI 96720 USA

¹²Kapteyn Astronomical Institute, Postbus 800, 9700 AV Groningen, The Netherlands

¹³Department of Astronomy, University of Texas, Austin, TX 78712, USA

¹⁴Institute for Advanced Study, Peyton Hall, Princeton, NJ 08544, USA

21 November 2021

ABSTRACT

Following our study on the incidence, morphology and kinematics of the ionised gas in early-type galaxies we now address the question of what is powering the observed nebular emission. To constrain the likely sources of gas excitation, we resort to a variety of ancillary data, we draw from complementary information on the gas kinematics, stellar populations and galactic potential from the SAURON data, and use the SAURON-specific diagnostic diagram juxtaposing the [O III] $\lambda 5007/H\beta$ and [N I] $\lambda\lambda 5197, 5200/H\beta$ line ratios. We find a tight correlation between the stellar surface brightness and the flux of the $H\beta$ recombination line across our sample, which points to a diffuse and old stellar source as the main contributor of ionising photons in early-type galaxies, with post-asymptotic giant branch (pAGB) stars being still the best candidate based on ionising-balance arguments. The role of AGN photoionisation is confined to the central $2'' - 3''$ of a handful of objects with radio or X-ray cores. OB-stars are the dominant source of photoionisation in 10% of the SAURON sample, whereas for another 10% the intense and highly-ionised emission is powered by the pAGB population associated to a recently formed stellar subcomponent. Fast shocks are not an important source of ionisation for the diffuse nebular emission of early-type galaxies since the required shock velocities can hardly be attained in the potential of our sample galaxies. Finally, in the most massive and slowly- or non-rotating galaxies in our sample, which can retain a massive X-ray halo, the finding of a spatial correlation between the hot and warm phases of the interstellar medium suggests that the interaction with the hot interstellar medium provides an additional source of ionisation besides old UV-bright stars. This is also supported by a distinct pattern towards lower values of the [O III]/ $H\beta$ ratio. These results lead us to investigate the relative role of stellar and AGN photoionisation in explaining the ionised-gas emission observed in early-type galaxies by the Sloan Digital Sky Survey (SDSS). By simulating how our sample galaxies would appear if placed at further distance and targeted by the SDSS, we conclude that only in very few, if any, of the SDSS galaxies which display modest values for the equivalent width of the [O III] line (less than $\sim 2.4\text{\AA}$) and LINER-like [O III]/ $H\beta$ values, the nebular emission is truly powered by an AGN.

Key words: galaxies : elliptical and lenticular – galaxies : ISM – galaxies : active

1 INTRODUCTION

If more than 30 years of investigations have now asserted the common presence of ionised gas in early-type galaxies (e.g. Caldwell 1984; Phillips et al. 1986; Kim 1989; Shields 1991; Goudfrooij et al. 1994; Macchetto et al. 1996; Sarzi et al. 2006), the sources powering the observed nebular emission have still to be firmly identified. As already revealed by the spectroscopic survey of Phillips et al. (1986), in early-type galaxies the ionised-gas emission show values for several line ratios that are generally consistent to what observed in low-ionisation nuclear regions, or LINERs (Heckman 1980). Since the nature of LINER activity in itself is somehow controversial (see Ho 2008, for a review), it is perhaps no surprise that the excitation mechanism for the extended LINER-like emission is still not known. In fact, in addition to the two most touted sources for LINER activity, a central AGN or fast shocks, the interaction with the hot phase of the interstellar medium (Sparks, Macchetto, & Golombek 1989) and photoionisation by old UV-bright stellar sources (Binette et al. 1994) have also been suggested as mechanisms for powering the nebular emission of early-type galaxies. The importance of these last two ionising source was highlighted by the narrow-band survey of Macchetto et al. (1996) and further stressed by the spectroscopic observations of Goudfrooij (1999), albeit only in the case of giant and dusty elliptical galaxies.

In this context, the SAURON integral-field survey (de Zeeuw et al. 2002) allowed a more systematic spectroscopic study of the ionised gas in nearby early-type galaxies, to an unprecedented sensitivity limit. In Sarzi et al. (2006, hereafter Paper V) we reported an amazing variety for the value of the $[\text{O III}]\lambda 5007/\text{H}\beta$ ratio both across the SAURON sample and within single galaxies, which suggests that a number of mechanisms is responsible for the gas excitation in early-type galaxies. If more than one source contributes to power the extended emission of early-type galaxies, disentangling their relative importance in nearby objects could prove critical also to understand the gas emission observed in distant galaxies by large-scale surveys such as the Sloan Digital Sky Survey (SDSS), where the nebular fluxes are integrated over large physical apertures. Yet, the limited wavelength range of the SAURON data (see Bacon et al. 2001) prevents the standard emission-line diagnostic that is routinely used to make a first assessment of the possible ionising sources (e.g., following Veilleux & Osterbrock 1987), so that other pieces of information are needed to tackle this problem. Presently, we can add to our emission-line measurements not only our knowledge of the gravitational potential of our sample galaxies (Cappellari et al. 2006, Paper IV) and of the basic properties of their stellar populations (Kuntschner et al. 2006, Paper VI), but we can also draw from a variety of ancillary data that have been collected and analysed over the course of the SAURON project. These range from GALEX ultraviolet images (Jeong et al. 2009), Spitzer infrared data (Shapiro et al. 2009) to mm- and cm- radio observations of the molecular and neutral gas (Combes, Young, & Bureau 2007; Morganti et al. 2006). Furthermore, for a minority of our sample galaxies it is possible to use a SAURON-specific diagnostic diagram that uses the $[\text{N I}]/\text{H}\beta$ line ratio as a gauge for the hardness of the ionising continuum. We are therefore in a unique position to start assessing the relative role of the various sources of ionisation that could be responsible to the nebular emission observed in early-type galaxies.

Our investigation will proceed as follows. In §2 we will introduce the potential of the $[\text{N I}]/\text{H}\beta$ diagnostic diagram and derive

more robust $[\text{N I}]$ measurements in order to maximise its use across our sample. In §3 we will review the importance of AGN activity, star formation, diffuse old stellar sources, fast shocks and of the interaction with the hot phase of the interstellar medium in powering the nebular emission observed across the SAURON sample. In §4 we will explore the implications of the lessons learnt in §3 for interpreting the ionised-gas emission observed in distant early-type galaxies that are targeted by large-scale spectroscopic survey such as the SDSS, and finally draw our conclusions in §5.

2 SAURON EMISSION-LINE DIAGNOSTICS

Emission-line diagnostic diagrams have had a long history of success in constraining the different sources of ionisation for the nebular emission observed in extra-galactic objects. Initially introduced by Baldwin, Phillips, & Terlevich (1981, hereafter BPT) to separate star-forming objects and active galactic nuclei (AGN), these diagrams juxtapose various emission-line ratios to provide a basis for classifying the gas emission into categories that, to varying degrees of confidence, can be identified with specific excitation sources. This is achieved by comparing the position of the data in the diagnostic diagrams with the predictions of sophisticated models for gas that is photoionised by a central AGN or by OB-stars (e.g., Ferland et al. 1998; Kewley et al. 2001) or that is excited by shocks (e.g., Dopita & Sutherland 1995, 1996). Today, the most widely adopted kind of BPT-diagrams are those introduced by Veilleux & Osterbrock (1987), who designed a diagnostic analysis that is insensitive to reddening and that is based on the ratios of strong emission lines rather close in wavelength, such as $\text{H}\beta$ $\lambda 4861$ and $[\text{O III}]\lambda\lambda 4959, 5007$ or $[\text{O I}]\lambda 6300$, $[\text{N II}]\lambda\lambda 6548, 6583$, $\text{H}\alpha$ $\lambda 6563$, and $[\text{S II}]\lambda\lambda 6716, 6731$.

Among the emission lines that usually feature in these diagrams only the $[\text{O III}]$ and $\text{H}\beta$ lines fall in the wavelength range of the SAURON spectra, which was intentionally restricted around the $\text{H}\beta$ and Mgb absorption-line features in order to measure the stellar kinematics and the properties of the stellar populations within the largest possible field of view. A traditional diagnostic analysis in our sample galaxies is therefore only possible when the SAURON data are complemented by integral-field observations in the $\text{H}\alpha+[\text{N II}]$ spectral region, as shown by Mazzuca et al. (2006) for the Sa galaxy NGC 7742.

2.1 The $[\text{N I}]$ lines and the $[\text{N I}]/\text{H}\beta$ diagnostic diagram

If standard BPT-diagrams cannot be drawn with SAURON data alone, the emission from the weak $[\text{N I}]\lambda\lambda 5197, 5200$ doublet allows for a diagnostic analysis that is rather similar to that normally carried out through the BPT-diagram based on the $[\text{O I}]/\text{H}\alpha$ line ratio. Indeed, similarly to the $[\text{O I}]$ emission also the $[\text{N I}]$ lines arise in partially ionised regions, which are extended in gaseous nebulae photoionised by a spectrum containing a large fraction of high-energy photons, but are almost absent in H II -regions. The $[\text{N I}]/\text{H}\beta$ ratio can therefore be used to gauge the hardness of the ionising continuum, making the $[\text{N I}]/\text{H}\beta$ vs. $[\text{O III}]/\text{H}\beta$ diagnostic diagram in principle as useful as the $[\text{O I}]/\text{H}\alpha$ vs. $[\text{O III}]/\text{H}\beta$ diagram to separate photoionisation by OB-stars from other excitation sources.

This is demonstrated by Fig. 1, which shows that the predictions of the MAPPING-III models in the event of a starburst, of gas photoionised by a central AGN and of gas excited by shocks (from Dopita et al. 2000; Groves, Dopita, & Sutherland 2004; Allen et al. 2008, respectively) are as well separated in the SAURON $[\text{N I}]/\text{H}\beta$

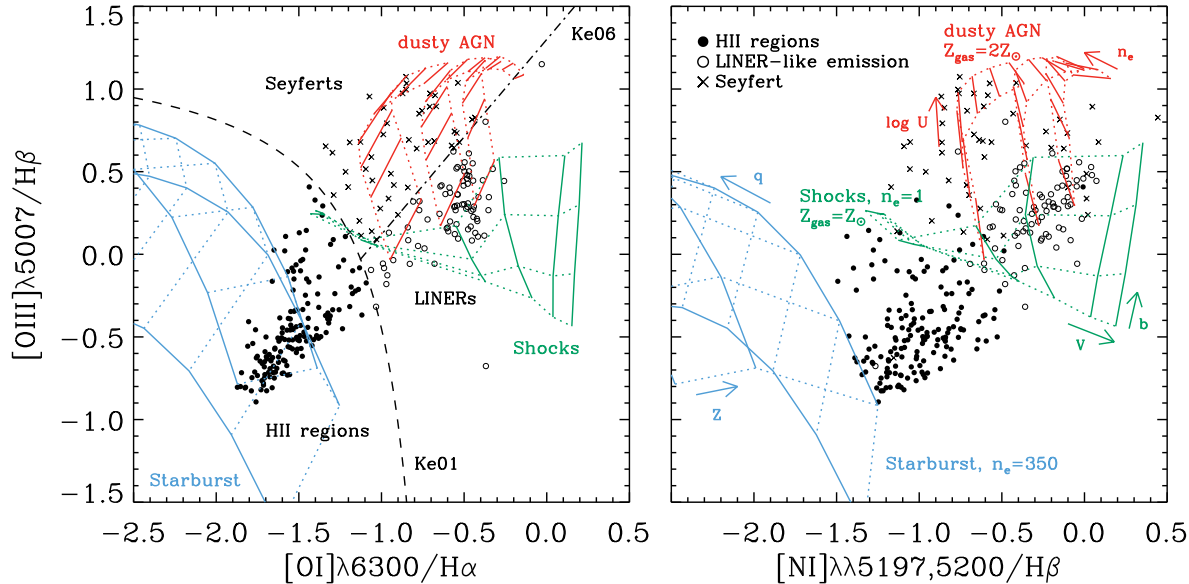


Figure 1. The standard [O I]/H α vs. [O III]/H β BPT diagram of Veilleux & Osterbrock (left) compared to the SAURON [N I]/H β vs. [O III]/H β diagnostic (right). In both panels the red, blue and green lines show the predictions of the MAPPINGS-III models for gas that is photoionised by a central AGN, by O-stars, or that is excited by shocks, respectively. The AGN grids are from the dusty, radiation pressure-dominated models of Groves, Dopita, & Sutherland (2004) and adopt three values for the index α of the power-law AGN continuum $f_\nu \propto \nu^\alpha$ ($\alpha = -1.7, -1.4, -1.2$ from left to right). In each AGN model grid the solid lines trace the dimensionless ionisation parameter $\log U$ (defined as $\log q/e$), which increases with the [O III]/H β ratio from $\log U = -3.0, -2.6, -2.3, -2.0, -1.6, -1.3, -1.0$, whereas the dotted lines show the adopted values for the electron density of $N_e = 10^2$ and 10^4 cm^{-3} , with smaller values of the [N I]/H β ratio corresponding to larger N_e values. The starburst grids are from Dopita et al. (2000), and assume a gas density of $N_e = 350 \text{ cm}^{-3}$ and use a spectral energy distribution obtained from Starburst99 (Leitherer et al. 1999) models for an instantaneous star-formation episode. The grids assume a range of metallicity Z for both stars and gas in the starburst, shown by the solid lines for $Z = 0.2, 0.4, 1.0, 2.0 Z_\odot$, and different values of the ionising parameter q , shown by the dotted lines for $q = 0.5, 1, 2, 4, 8, 15, 30 \times 10^7 \text{ cm s}^{-1}$. Similarly, for the shock grids (without precursor H II region), the solid lines show models with increasing shock velocity $V_s = 150, 200, 300, 500, 750, 1000 \text{ km s}^{-1}$, and the dotted lines models with magnetic parameter $b = 0.5, 1.0, 2.0, 4.0$. The shock grids are from Allen et al. (2008) and assume an electron density of $N_e = 1 \text{ cm}^{-3}$ and a solar value for the gas metallicity. In both panels the filled circles, the crosses and the open circles show the values of the emission-line ratios observed in the central $3''$ of 284 galaxies with SDSS spectra, where according to the limits draw by Kewley et al. (2001) and Kewley et al. (2006) in the [O I]/H α diagram the nebular emission is most likely arising from H II regions, from a Seyfert AGN or from LINER-like emission regions, respectively.

diagnostic as they are in the standard [O I]/H α BPT diagram. In Fig. 1 we also show the distribution of the emission-line ratios measured with the method of Paper V in the central regions of 284 galaxies observed by the Sloan Digital Sky Survey (SDSS). This sample includes all galaxies with SDSS spectra (from the DR6 release), not only early-type galaxies, with redshifts between $0.02 < z < 0.05$, apparent r -band magnitude brighter than $r < 16$ and, most important, with detected [N I] emission. If we adopt the conservative theoretical limit of Kewley et al. (2001) to identify star-bursting SDSS galaxies in the [O I]/H α BPT diagram and further separate Seyfert nuclei from objects showing LINER-like central emission using the empirical line drawn by Kewley et al. (2006), Fig. 1 illustrates how these three kinds of objects are clearly separated also in the SAURON [N I]/H β diagnostic diagram.

The position of the SDSS galaxies displaying nuclear star formation and LINER-like emission in Fig. 1 deserves further attention. Starting with the star-forming galaxies, the fact that the MAPPINGS-III starburst models systematically underpredict the values of the [N I]/H β ratio suggests that, similarly to case of the [O I] line (Stasińska & Leitherer 1996; Dopita et al. 2000), also the [N I] fluxes can be significantly enhanced by the mechanical energy released by supernovae and stellar winds, which are naturally expected in starbursts as a result of stellar evolution. As regards the location of the SDSS galaxies exhibiting central LINER-like emis-

sion, we note that these objects are more clearly separated from the Seyfert nuclei in the [N I]/H β diagnostic diagram than they are in the [O I]/H α diagram. Furthermore, most of the SDSS LINER nuclei appear to follow a tight sequence consistent with photoionisation by a central AGN with increasingly harder ionising radiation fields, in agreement with the findings of Kewley et al. (2006) based on the [O I]/H α diagnostic. These results further stress the usefulness of the [N I] lines as a gauge for the hardness of the ionising continuum.

Unfortunately, the 2nd and 3rd energy levels of neutral Nitrogen have a much smaller critical de-excitation density (7×10^2 and $2.2 \times 10^3 \text{ cm}^{-3}$) than the 4th level of neutral Oxygen ($1.5 \times 10^6 \text{ cm}^{-3}$), so that the [N I] lines are generally much fainter than the [O I] line owing to collisional de-excitation. The SAURON [N I]/H β diagnostic diagram is therefore applicable only in the few early-type galaxies where nebular emission is particularly intense. To complicate matters further, as discussed in Paper V the detection of the [N I] lines is hampered by our limited ability to match the underlying continuum in the spectral region around the Mg b absorption features.

2.2 Improving the [N I] measurements with the MILES spectral library

In Cappellari et al. (2007, Paper X) we re-extracted the stellar kinematics for our sample galaxies using for each galaxy a different subset of stellar templates from the MILES library of Sánchez-Blázquez et al. (2006). The MILES templates provide a much better fit to the emission-free spectral regions of our data, and thus their use delivers a more reliable stellar kinematics.

In an attempt to further improve the extent and quality of our [N I] measurements, we re-extracted also the nebular emission fluxes and kinematics using the MILES stellar library. In the case of emission-line measurements, however, it is crucial to provide an underlying fit to the stellar continuum that is as physically motivated as possible in order to avoid spurious results. For this reason, rather than using a subset of stellar spectra from the MILES library for each galaxy as done in Paper X, we used a template library consisting of simple stellar population models from Vazdekis et al. (2009, based on MILES stellar spectra, see also Vazdekis et al. 2007) to which we added a number of empirical templates obtained by matching real SAURON spectra, most of the times devoid of emission.

Specifically, based on the maps of Paper V for the ionised-gas emission, we extracted a number of high-S/N SAURON spectra from circular apertures in galactic regions either without significant emission or with emission lines that were clearly distinguishable from the underlying absorption spectrum, which we fitted over the *entire* wavelength range with the MILES stars (excluding stellar templates with exceedingly low values of the $H\beta$ absorption-line strength). The optimal combination of the stellar spectra that best matched each of our emission-free aperture spectra constitute each of the empirical templates in our new template library. Care was taken to extract SAURON spectra covering the distribution of the absorption-line strengths observed in Paper VI, which cannot be covered in detail by the distribution of line-strengths values measured in the MILES stellar library since this consists mostly of spectra for nearby stars. In this respect, our empirical templates approximate as closely as possible the spectra of real early-type galaxies, were they unaffected by kinematic broadening. Fig. 2 illustrates the poor coverage that the MILES stellar library provides for the absorption-line strengths observed in early-type galaxies, in particular in the plane defined by the Mgb and $Fe5015$ indices, which the adopted array of single stellar population models and empirical templates can match in a more physical manner.

Compared to the fit of Paper V, the use of such a mixed library of model and empirical templates based on MILES stellar spectra leads to a significant increase in the quality of the fit to the SAURON spectra in the Mgb region (corresponding to a 30% decrease in the RMS of the fit residuals), which adds confidence in the [N I] measurements. In general the $H\beta$ and [O III] measurements obtained with the new set of templates do not differ significantly from our previous measurements, which reflect the modest 10% decrease in the RMS of the fit residual when the entire SAURON wavelength range is considered. Therefore, for the sake of clarity hereafter we will quote and plot the $H\beta$ and [O III] measurements from Paper V, and use the newly extracted emission-line measurements only when discussing the [N I]/ $H\beta$ diagnostic diagrams or when comparing maps for the [N I] and $H\beta$ emission.

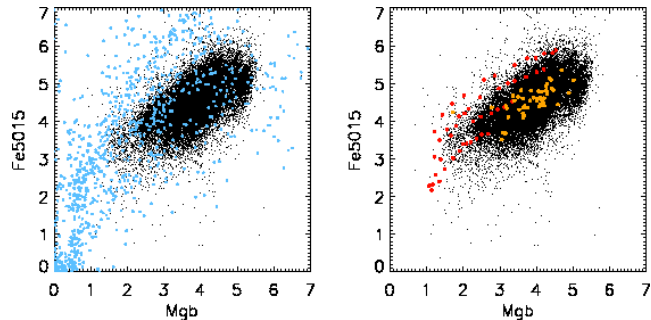


Figure 2. Distribution of the values for the Lick Mgb and $Fe5015$ indices observed across the SAURON sample (from the maps of Paper VI, black dots) compared to that observed across the MILES stellar library (left, blue circles) or for the single-age models of Vazdekis et al. and the empirical templates based on matching real SAURON spectra (right, red and orange circles, respectively). The MILES stars provide a poor coverage of the region in the Mgb vs. $Fe5015$ plane that is most populated by the SAURON data, which causes the continuum fit process to adopt unphysical combinations of stars and thus leads to spurious emission-line measurements, in particular to exceedingly large [N I] fluxes. This is not the case when simple stellar population models and empirical templates are adopted, although the quality of the fit is formally not as good.

3 IONISATION SOURCES

Except for very low and high values of the [O III]/ $H\beta$ ratio that most likely correspond to H II-regions and Seyfert nuclei, respectively, the diagnostic diagrams of Fig. 1 illustrate vividly how without other line ratios than [O III]/ $H\beta$ it is impossible to immediately separate star formation from AGN activity. Besides, a number of ionising mechanisms in addition to AGN activity, such as fast shocks (Dopita & Sutherland 1995), photoionisation by old stars (Binette et al. 1994) and the interaction with the hot, X-ray emitting gas (Sparks, Macchetto, & Golombek 1989), have been suggested to explain the emission in the $\log([O III]/H\beta) = 0 - 0.5$ range, which is typical of LINER-like emission (e.g., Ho, Filippenko, & Sargent 1997) and that includes 75% of [O III]/ $H\beta$ values observed across the SAURON sample. In fact, very low [O III]/ $H\beta$ values are observed also in the absence of star formation, for instance in the X-ray filaments around the brightest galaxies of clusters (e.g., Hatch et al. 2006; Sabra, Shields, & Filippenko 2000), whereas quite large [O III]/ $H\beta$ ratios can be observed also in H II-regions if the metallicity is extremely low.

For this reason in this section we will use a variety of ancillary data, ranging from radio to X-ray wavelengths, and consider complementary information on the gas morphology and kinematics from our SAURON data to constrain the most likely sources of gas excitation in different kind of galaxies, using, when possible, the [N I]/ $H\beta$ diagnostic to corroborate our findings.

3.1 Nuclear Activity

Many of our sample galaxies host AGNs. Well-known cases include NGC 4486 and NGC 4374 for their FR I radio jets (e.g., Owen et al. 1989; Laing & Bridle 1987), NGC 4278 for hosting a well-studied LINER nucleus (e.g., Goudfrooij et al. 1994; Giroletti, Taylor, & Giovannini 2005) and NGC 4552 for an ultraviolet flare that could have resulted from the tidal stripping of a star passing close to the central black hole (Renzini et al. 1995; Cappellari et al. 1999)

Given that unresolved radio-continuum cores are excellent

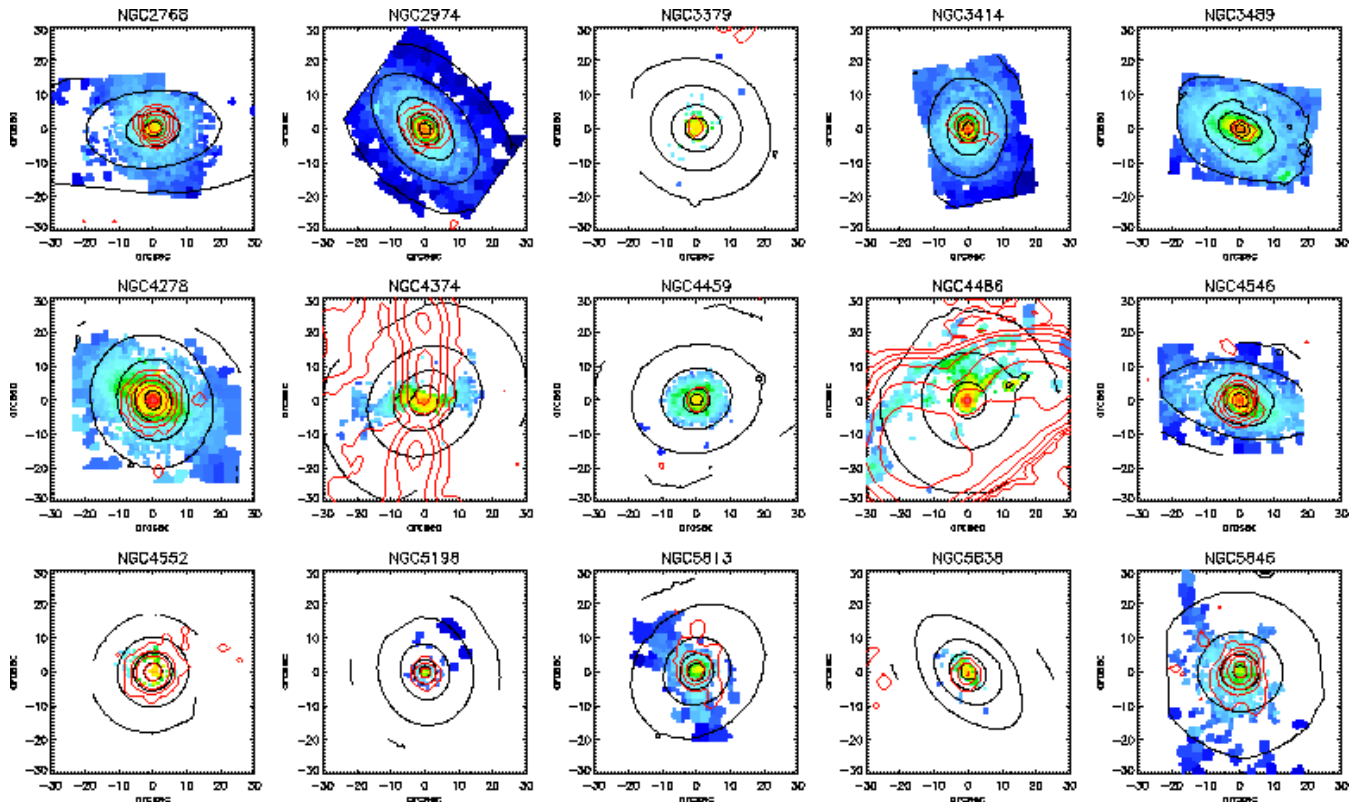


Figure 3. SAURON $H\beta$ emission vs. VLA measurements for the 1.4 GHz radio continuum from the FIRST survey and for galaxies with compact radio cores. As in Paper V the $H\beta$ fluxes are colour-coded in a logarithmic scale with values ranging between 10^{-14} and 10^{-18} $\text{erg s}^{-1} \text{cm}^{-2} \text{arcsec}^{-2}$. The red contours show the 1.4 GHz fluxes also in logarithmic scale, starting from a level of 0.45 mJy/beam (corresponding to 3 times the typical RMS of the FIRST images) and doubling with each contour, except for NGC 4278, NGC 4374, NGC 4486 and NGC 4552 for which the 1.4 GHz fluxes changes by a factor 5 between each line. The beam of the FIRST images is circular and has a FWHM of $5''.4$.

signposts for black-hole accretion, in this section we focus on the galaxies in our sample that exhibit such a feature. In the area covered by the VLA FIRST survey (Becker, White, & Helfand 1995) there are 15 galaxies with 1.4 GHz compact cores. Figure 3 compares the SAURON $H\beta$ emission with the distribution of the 1.4 GHz radio continuum, which in several cases extends beyond the nucleus. In particular, a comparison with the beam of the FIRST images reveals that the nuclear emission is resolved in NGC 2974, NGC 3414, NGC 4546, NGC 5813 and NGC 5846, while in NGC 3489 the radio core is only marginally extended.

Among the SAURON galaxies that have not been observed by the FIRST survey, the presence of a radio core has been excluded in NGC 474 and NGC 821 by Wrobel (1991) and in NGC 7457 and NGC 7332 by Morganti et al. (2006). The remaining galaxies, NGC 524 and NGC 1023, do host a radio core according to Filho et al. (2004) and Morganti et al., respectively. In what follows we will use the radial profiles for the values of the $H\beta$ flux and the $[\text{O III}]/H\beta$ ratio to understand the extent to which AGN can power the nebular emission in our sample galaxies. In particular, it will be shown that extremely shallow $H\beta$ and $[\text{O III}]/H\beta$ are inconsistent with AGN photoionisation. This is the case of NGC 524, whereas for NGC 1023 the absence of central $H\beta$ emission precludes any further analysis. Conversely, among the objects with undetected radio-continuum cores in the FIRST images, NGC 4477 display a strong and unresolved central $H\beta$ peak and a very steep $[\text{O III}]/H\beta$ gradient, suggesting that AGN photoionisation is important toward the centre of this galaxy. The presence of a powerful

AGN in NGC 4477 is signalled by a strong X-ray nucleus (first detect by the *Einstein* observatory by Fabbiano, Kim, & Trinchieri 1992), and its radio-quiet nature is consistent with its Seyfert classification (Ho et al. 1997; Ho 2008).

If we assume a uniform gas density and constant filling factor for gas clouds residing on a plane, in ionisation equilibrium the surface brightness of the $H\beta$ recombination line should follow the strength of the radiation field, therefore radially decreasing as r^{-2} in the case of a central source. The strength with which the AGN radiation reaches the gas clouds, usually quantified by the ionisation parameter q that compares the ionising-photon and electron density at the face of the irradiated cloud, also determines the ionisation state of the gas clouds. For our purposes the $[\text{O III}]/H\beta$ ratio is an excellent diagnostic for the ionisation state of the gas, not only since this ratio involves emission from a highly-ionised species (e.g., Ferland & Netzer 1983; Ho, Shields, & Filippenko 1993) but also because the $[\text{O III}]/H\beta$ ratio scales almost linearly with q for the range of values observed in the SAURON nuclei (i.e., for $[\text{O III}]/H\beta \leq 5$). Therefore, also the values of the $[\text{O III}]/H\beta$ ratio should follow a r^{-2} profile under the previous assumptions.

On the other hand, if the gas density decreases with radius, the $H\beta$ surface brightness will drop at an even faster gradient than inverse-square, whereas the $[\text{O III}]/H\beta$ ratio will display a shallower radial profile as the ionisation parameter q decreases more gently with radius. Furthermore, if the gas is also vertically extended rather than just being distributed in a planar configuration, projection effects will lead to shallower $H\beta$ surface brightness pro-

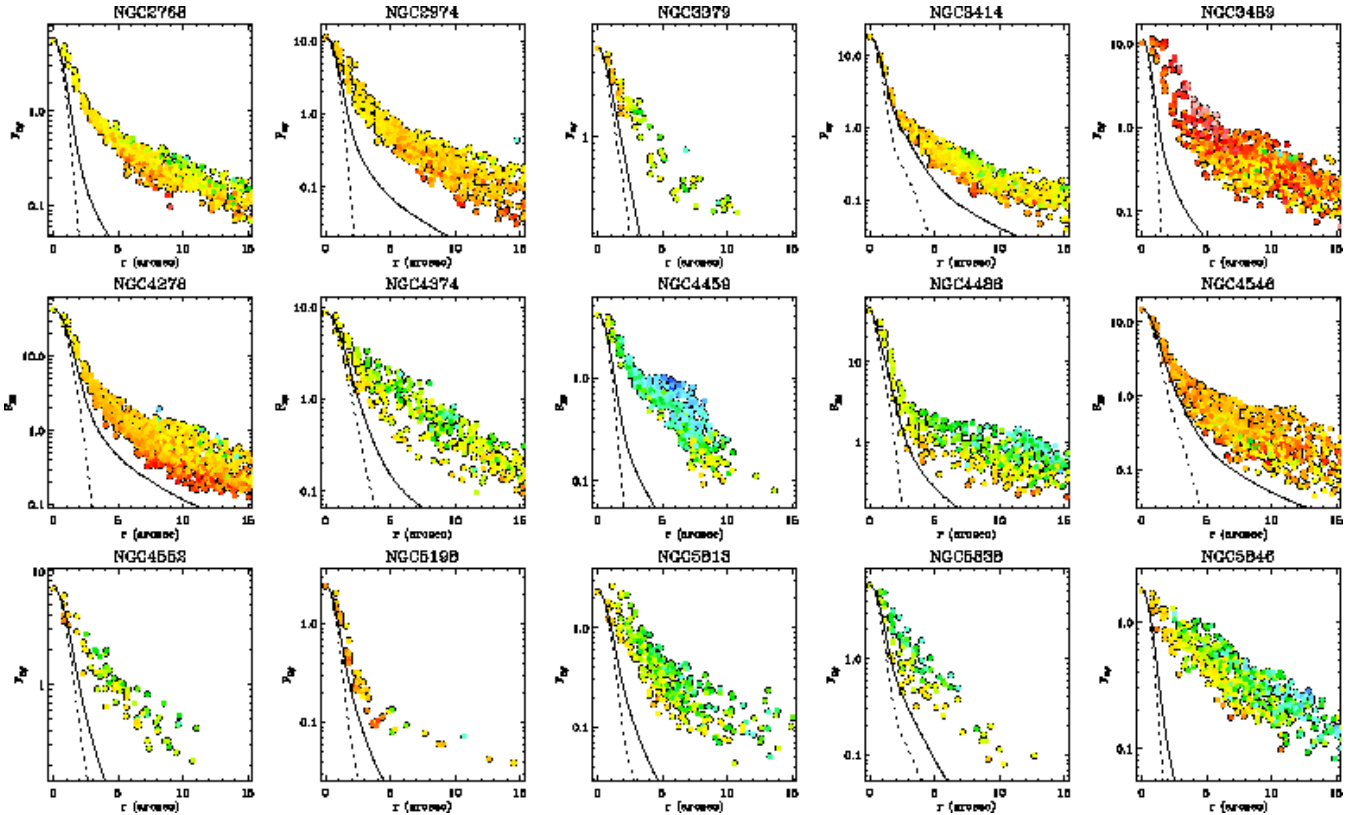


Figure 4. Radial profiles for the $H\beta$ flux values in galaxies with 1.4 GHz radio cores. The $H\beta$ fluxes are in units of $10^{-16} \text{ erg s}^{-1} \text{ cm}^{-2} \text{ arcsec}^{-2}$ and are plotted only out to $15''$. In each panel the solid line shows the r^{-2} radial decrement that is expected in the case AGN photoionisation and under the special conditions of constant gas density and filling factor, accounting for the impact of atmospheric blurring. The point-spread function of the SAURON observations, from Paper III, is shown by the dotted lines. Both profiles have been normalised to the central $H\beta$ emission. The $H\beta$ data are colour-coded according to the logarithm of the $[\text{O III}]/H\beta$ ratio, going from blue to green and red for values of -1, 0 and 1.

files. In this case the $[\text{O III}]/H\beta$ values will follow the same trend as the $H\beta$ emission and also show a gentler radial decline, as clouds at different distances from the centre and hence subject to different ionising photon densities are observed along the same line of sight. Conversely, if the gas clouds lie in a plane, the AGN radiation could be absorbed by intervening material before reaching the gas clouds at any given radius, leading to $H\beta$ and $[\text{O III}]/H\beta$ profiles that are steeper than an r^{-2} law. Finally, radial gradients in the filling factor of the gas clouds will only affect the $H\beta$ surface-brightness profiles, in the same direction as variations in the gas density would do.

Figure 4 plots the radial profile of the $H\beta$ emission in the SAURON galaxies with 1.4 GHz radio cores, together with the predicted r^{-2} radial decrement for AGN photo-ionisation and under the special conditions of constant gas density and filling factor, accounting for atmospheric blurring. The $H\beta$ data-points in Fig. 4 are colour-coded according to the value of the $[\text{O III}]/H\beta$ ratio, in order to convey also the radial variation of this quantity. Figure 4 shows that the surface brightness profile of the $H\beta$ emission is in keeping with our simplest expectations for AGN photo-ionisation only in the very central regions of a few objects (e.g., NGC 3414, NGC 4278, NGC 4546) whereas in general the $H\beta$ profile is shallower than an inverse-square law, in particular beyond the central $\sim 3''$. The behaviour of the $[\text{O III}]/H\beta$ ratio, which does not appear to systematically decrease with radius, further rules out a central AGN as the source of ionisation for the gas emission beyond the innermost regions of our sample galaxies. In fact, that the $[\text{O III}]/H\beta$

ratio tends to display rather constant values in the innermost regions (within 20% of the average within $3''$, see also Fig. 4b of Paper V) suggests that if an AGN is responsible for the gas excitation where the $H\beta$ surface-brightness profile is consistent with a r^{-2} law, then the assumptions of our simplest scenario cannot hold. In this respect, we note that if the central gas of our sample galaxies has settled on a steady disk, this should display a radially decreasing profile for the column density (Kawata, Cen, & Ho 2007), which is proportional to the gas density and the filling factor of the gas clouds. The presence of a negative gradient for the gas density could address the need for shallow $[\text{O III}]/H\beta$ profiles in the nuclear regions of galaxies with $H\beta$ gradients that are consistent with the inverse-squared model, even though a radially decreasing gas density would induce even steeper $H\beta$ gradients. Indeed, such a change could not be appreciated by our observations as those central $H\beta$ profiles are in fact unresolved. On the other hand, if we were to advocate the role of AGNs also where the $H\beta$ surface-brightness profile is resolved and is slightly shallower than an r^{-2} law (e.g., NGC 2768, NGC 2974, NGC 4486) then projection effects would have to be invoked in addition to a radial decrement of the gas density. Considering vertically extended structures may also help to explain some of the sharpest peaks for the value of the gas velocity dispersions that are observed in our sample (e.g., NGC 3414, NGC 4278, NGC 5198).

As a final item of this section, in Fig. 5 we draw the $[\text{N I}]/H\beta$ vs. $[\text{O III}]/H\beta$ diagnostic diagram for the ionised-gas

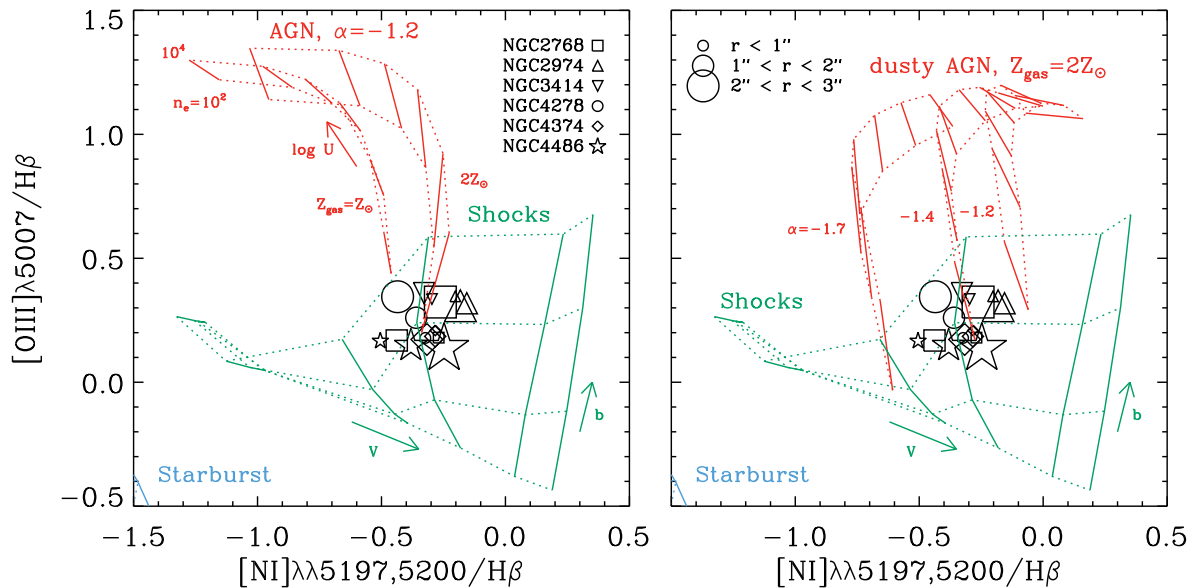


Figure 5. SAURON [N I]/H β vs. [O III] λ 5007/H β diagnostic diagram for galaxies with 1.4 GHz radio cores. The different symbols correspond to each of the galaxies with detected [N I] emission, and the size of the symbols indicate the radial range over which the average values of the [N I]/H β and [O III]/H β ratios have been computed. The colored grids show the same MAPPINGS-III models as in Fig. 1, except for the AGN photoionisation models shown in the left panel, which do not include dust, correspond to a single value of the power-law index of the AGN continuum of $\alpha = -1.2$ and are shown also for solar values of the gas metallicity. The range of the dimensionless ionising parameter of the dust-free AGN models is also somewhat different, including values of $\log U = -3.3, -3.0, -2.6, -2.3, -2.0, -1.6$.

emission observed in the central 3'' of the SAURON galaxies with 1.4 GHz radio-continuum cores and [N I] emission. The emission in the central regions of these objects is generally consistent with both photoionisation from a central AGN with a very low ionisation parameter and with excitation from fast shocks. If we disregard the latter possibility for the moment (see §3.4), we note that only models including gas of super-solar metallicity and a self-consistent treatment of dust (Dopita et al. 2002; Groves, Dopita, & Sutherland 2004) provide a plausible description for our data. In particular, dust-free models with gas of solar metallicity (Fig. 5, left) can match just a fraction of our data (e.g., the very center of NGC 4486) and only with the hardest ionising radiation fields (i.e., $f_\nu \propto \nu^{-1.2}$). Super-solar values for the gas metallicity are required also in the case of dusty, radiation pressure-dominated photoionization (Fig. 5, right), since also these models would have to invoke the hardest ionising continuum in order to match our data in the case of gas of solar metallicity (not shown for the sake of clarity). The very nuclear regions of the objects in Fig. 5 (within 1'', smallest symbols) appear consistent with dusty super-solar AGN models while adopting similarly low values of the ionisation parameter and a realistic range for the hardness of the AGN radiation field (from $f_\nu \propto \nu^{-1.7}$ to $\nu^{-1.2}$), in keeping with the behaviour of the SDSS LINER nuclei (§2.1). Figure 5 shows that significant radial variations in the average values of the [N I]/H β and [O III]/H β ratios are found only in NGC 2768, NGC 4278 and NGC 4486. As the average values of the line ratios do not run parallel to the dusty AGN models, such gradients are inconsistent with a simple radial change in the mean value of the ionising parameter (due to either a different mean distance or gas density) or of the gas density, suggesting instead a variation in the hardness of the AGN radiation field. This seems rather unlikely, however, in particular for NGC 4486 where the radial increase of the [N I]/H β ratio would imply a hardening of

the AGN continuum hitting clouds at increasing distance from the centre. Therefore, excluding the possibility of special gas and dust geometries, we consider it more likely that other processes than AGN photoionisation are responsible for the gas excitation beyond the very centre of these objects. In fact, for NGC 4486 the results of Sabra et al. (2003) and Dopita et al. (1997) suggest a radial transition from nuclear AGN photoionisation to circumnuclear gas excited by fast shocks.

To conclude, the presence of a 1.4 GHz radio-continuum core suggests that a central AGN could be responsible for powering the ionised-gas emission in the very centre of 30% of our SAURON sample galaxies, at most. For AGN photoionisation to be consistent with the observed radial profiles of the [O III]/H β line ratio within the central 3'', the central gas distribution has to have a radially decreasing density, and in the case of objects with resolved H β emission profiles, also a vertically extended structure. Even so, the presence in few objects of considerable gradients in the value of [N I]/H β ratio suggests that other mechanisms than photoionisation by a central AGN must contribute to power the nebular emission outside the very centre.

3.2 H II-regions

A few early-type galaxies in the SAURON sample show clear evidence of on-going star-formation. In particular, the values of the [O III]/H β ratio in NGC 3032, NGC 4526, NGC 4459 plunge to levels that are well below the lower-limit of the [O III]/H β ratio that is observed also in LINER-like emission regions and Seyfert nuclei, which is around [O III]/H $\beta \sim 0.3$ or $\log([O III]/H\beta) = -0.5$ (see, e.g., Kewley et al. 2006). As noticed already in Paper V, these objects are also characterised by extremely regu-

lar dust morphologies and gas kinematics, in particular that of the $H\beta$ line, suggesting a relaxed gas distribution and dynamics. Similarly relaxed structures are observed also in NGC 524 and NGC 5838, which too show low $[O III]/H\beta$ values although never down to the low level that is observed in the previous galaxies. That star formation may be occurring in NGC 3032, NGC 4459, and NGC 4526 is supported also by the finding of massive disks of molecular gas (Combes, Young, & Bureau 2007; Young, Bureau & Cappellari 2007) and the detection of emission from polycyclic aromatic hydrocarbons (PAHs Shapiro et al. 2009).

Yet, even in these relatively simple objects we observe strong gradients in the value of the $[O III]/H\beta$ ratio, which underscore the presence of other sources of ionisation than OB-stars. In this respect it is useful to observe in Fig. 6 the behaviour in the $[N I]/H\beta$ diagnostic diagram of the SAURON data for NGC 3032 and NGC 4526, the only two star-forming early-type galaxies with detected $[N I]$ emission. For comparison, in Fig. 6 we also show the same SAURON measurements for the Sa galaxy NGC 4314 (from Falc3n-Barroso et al. 2006), which hosts a central star-forming ring and where the nebular emission is stronger, in terms of equivalent width of the lines, than in NGC 3032 and NGC 4526. Figure 6 confirms dramatically the presence of star formation in NGC 3032 and NGC 4526 as it shows that the SAURON measurements in these two objects display the same characteristic diagonal trend in the $[N I]/H\beta$ vs. $[O III]/H\beta$ diagram that is observed also in SDSS galaxies with star-bursting nuclei (Fig. 1) and in the ring of NGC 4314. Furthermore, Fig. 6 confirms the impression conveyed by the maps for the equivalent width of the $H\beta$ emission (Fig. 4b of Paper V) that, as in the case of NGC 4314, star formation in NGC 3032 and NGC 4526 occurs primarily in a ring. Indeed, in Fig. 6 the SAURON data reveal a striking similarity between the line-ratio gradients observed in NGC 3032, NGC 4526 and the Sa NGC 4314, whereby in all three galaxies the emission-line properties move closer to the predictions of the dusty AGN or shock models as we consider regions away from the star-forming ring *both* towards the centre and the outer regions of the galaxy. In fact, in NGC3032 the regions outside the ring seem to approach the AGN and shock grids from a different direction than the points inside the ring, which would suggest either that toward the centre AGN photoionisation is more important than shock excitation, or that shocks may occur under different conditions at the opposite edges of the ring. A similar trend was observed also by Mazzuca et al. (2006) in the Sa galaxy NGC 7742 using standard BPT diagrams.

In Fig. 6 we also overplot on the SAURON maps the contour corresponding to the 1.4 Ghz radio-continuum emission measured by the FIRST survey. Consistent with synchrotron radiation from relativistic electrons and free-free emission from H II regions, the radio continuum is resolved and matches well the distribution of the nebular emission. Similarly to the case of normal disk galaxies (Kennicutt 1983), the 1.4 Ghz emission in NGC 3032 and NGC 4526 is dominated by the non-thermal synchrotron component, given that the thermal free-free emission that would correspond to our $H\beta$ fluxes falls short to explain the observed flux density values. In fact, following the prescription of Condon (1992) and Caplan & Deharveng (1986) to convert the $H\beta$ emission into free-free emission, the observed 1.4 Ghz flux densities appear remarkably consistent with our SAURON emission-line measurements (accounting for beam smearing) if we adopt a 10% fraction for the thermal component to the total 1.4 Ghz fluxes, as found on average in disk galaxies (Kennicutt 1983). That also in early-type galaxies the 1.4 Ghz continuum traces mostly the synchrotron

emission may explain why in Fig. 6 the radio contours do not appear to follow in detail the $H\beta$ emission observed in NGC 3032 and in the Sa NGC 4314, in particular where the $H\beta$ fluxes peak. Judging the agreement between radio and nebular emission is more difficult in NGC 4526, due to the higher inclination of its gaseous disk. It is instructive to note also the different impact of reddening by dust in NGC 3032 and NGC 4526 due to inclination effects, which explains why the latter galaxy shows brighter radio continuum flux densities, which are unaffected by dust, despite displaying fainter $H\beta$ emission.

No diffuse radio emission is detected in the rings of NGC 4459 and NGC 524, due to the fact that the nebular emission in these objects is significantly fainter than that observed in NGC 3032 and NGC 4526, and the corresponding radio emission has escaped detection in the FIRST images. Given the typical detection threshold of 0.45 mJy/beam in the FIRST survey, we expect to detect radio emission associated to star-formation in the FIRST images only if the average surface brightness of the $H\beta$ line within 99.73% of the FIRST beam ($FWHM=5''.4$) exceeds $\sim 0.9 \times 10^{-16} \text{ erg cm}^{-2} \text{ s}^{-1} \text{ arcsec}^{-2}$, including also the contribution of synchrotron emission. This level of surface brightness for the $H\beta$ line (conveniently shown in Fig. 4a of Paper V in light-green colours) is never achieved in the ring regions of NGC 524 and NGC 4459. On the other hand, the $H\beta$ and $[O III]$ flux values in NGC 5838 are comparable to what is measured in NGC 4526, suggesting that the unresolved 1.4 Ghz emission shown in Fig. 3 could arise from the compact gaseous disk of NGC 5838 as well as from a central AGN, in agreement also with the fact that this object sits on the far-IR to radio-continuum emission relation (Combes, Young, & Bureau 2007).

Could photoionisation by OB-stars be responsible also for the nebular emission that is observed in galaxies with less relaxed dust and gas structures or $\log([O III]/H\beta)$ values greater than -0.5 ? Star formation is unlikely to be the source of excitation for clouds with $\log([O III]/H\beta) > 0.5$, corresponding to starburst models with low metallicity and large q values (Fig. 1). Star formation episodes characterised by subsolar metallicity values are indeed extremely rare (because gas is quickly enriched during such events), whereas the ionisation parameter of extragalactic H II-regions is typically found to range only between $10^7 < q < 10^8$ (Dopita et al. 2000). For more intermediate values of the $[O III]/H\beta$ ratio, the possibility that OB-stars could be powering the observed emission is particularly compelling when there is evidence for recent star formation, for instance from the analysis of optical spectra (Paper VI and VIII) or of near-UV colours (e.g., Jeong et al. 2007), or in the presence of massive reservoirs of molecular gas (Combes, Young, & Bureau 2007). In this respect, cases like NGC 3489 and NGC 3156 are particularly intriguing (but see also §3.5). Both of the previous conditions are met in these objects, where the gas kinematics is also fairly relaxed with small values of the gas velocity dispersion σ_{gas} . Yet, despite these similarities with the star-forming objects, the $[O III]/H\beta$ ratio in NGC 3489 and NGC 3156 is consistently > 1 , peaking to remarkably high values (~ 10) in places well outside the nucleus, which rules out H II regions as the main source of nebular emission.

For these and other objects with evidence of recent star formation or reservoirs of molecular gas we can use the VLA FIRST radio-continuum data to further test whether the observed nebular fluxes are *entirely* associated to star formation activity. For instance, if the nebular emission observed in NGC 3489 was powered by OB-stars, following the previous prescription to derive 1.4 Ghz fluxes from the observed $H\beta$ emission, we should see a well resolved radio structure, as in the case of the star-forming

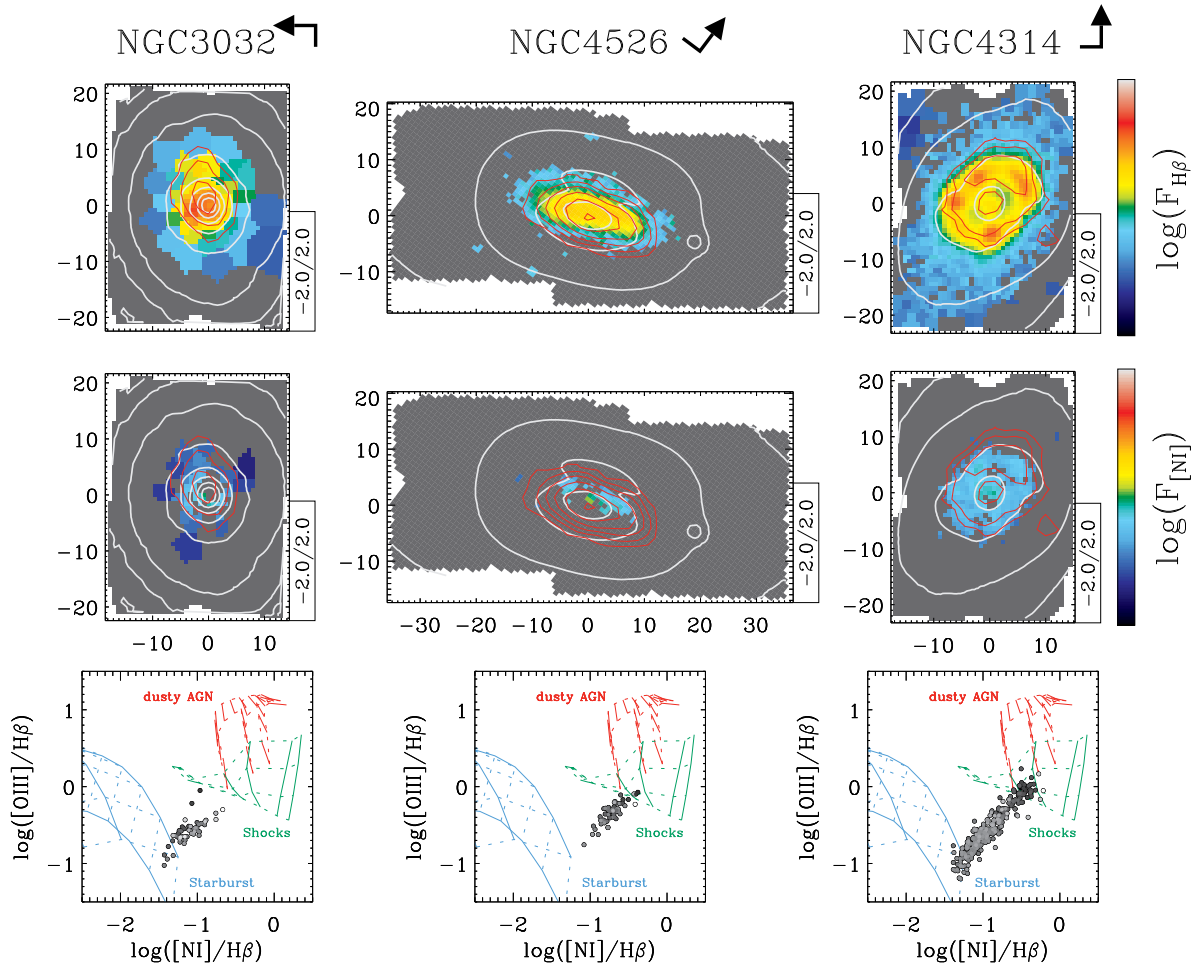


Figure 6. Two examples of lenticular galaxies with extremely regular dusty disks and gas kinematics where star formation is on-going, shown together to the Sa galaxy NGC 4314 which hosts a well-known circumnuclear star-forming ring. The top and middle panels show maps for the $H\beta$ and $[N\ I]\lambda\lambda 5198, 5200$ emission. Superimposed to these maps are 1.4 GHz radio continuum contours (red lines) from the FIRST-VLA images illustrating the resolved character of the synchrotron and free-free emission. As in the Paper V and for the SAURON maps in following figures, the white contours follow the stellar surface brightness, the scale is in arcsec and the side box show the range of the plotted quantity, in this case the flux of the $H\beta$ and $[N\ I]$ lines, in logarithmic scale. The $[N\ I]$ doublet is detected only where $[O\ III]$ and $H\beta$ emission is the strongest, which allows to trace these regions in $[N\ I]/H\beta$ diagnostic diagrams shown in the lower panels. Similar to the case of the most intense starburst observed in SDSS data (Fig. 1), all three galaxies share a distinct diagonal trend in the $[N\ I]/H\beta$ diagnostic, with the central and outermost regions (shown in darker and lighter points, respectively) departing the most from the starburst model grids and falling closer to the AGN or shock grids.

galaxy NGC 4526 that indeed displays similar values for the $H\beta$ fluxes. This is not observed, since NGC 3489 presents a rather weak and only marginally resolved core (§3.1) Similarly, in NGC 3156 the central $H\beta$ emission is sufficiently intense that if it were associated to star formation it would lead to a detectable radio core, but this is not observed. The non detection of 1.4 GHz radio-continuum features excludes the possibility that nebular emission is powered solely by OB-stars also in the nuclei of NGC 2685, NGC 4150 and NGC 7332, which have young stellar populations, relatively bright central $H\beta$ emission and, except for NGC 7332, also molecular gas. Among the objects with old stellar ages, as estimated from the SAURON absorption-line measurements, it is worth considering the cases of NGC 2768, which has a robust single-dish CO detection (Combes, Young, & Bureau 2007), and of NGC 2974, where the near-UV colours suggest the presence of young stars in the centre and in an outer ring (Jeong et al. 2007). Although both galaxies display strong radio-continuum cores

that are undoubtedly dominated by AGN activity, the observed $H\beta$ fluxes are sufficiently strong and extended (exceeding the $\sim 0.9 \times 10^{-16} \text{erg cm}^{-2} \text{s}^{-1} \text{arcsec}^{-2}$ threshold, Fig. 4) that if they were entirely powered by OB-star the corresponding free-free and synchrotron emission from star-forming regions would be capable of inducing noticeable and extended features in the radio-continuum maps. That in NGC 2768 the radio core is unresolved therefore suggests that star-formation cannot be principal the source of ionization in the central regions. Conversely, the fact that the radial profile for the 1.4GHz continuum in NGC 2974 is resolved does not necessarily imply that the $H\beta$ emission is powered by OB-stars. In fact, this possibility will be ruled out in §3.4 by means of the SAURON $[N\ I]/H\beta$ diagnostic, suggesting that the extended nature of the radio core of NGC 2974 may be due to the presence of an unresolved jet. Notwithstanding the lack of evidence for nuclear star formation, we note that NGC 2768 and NGC 2974 are among the brightest IRAS far-infrared sources

in our sample (together with NGC 524, NGC 3032, NGC 4459, NGC 4526 and NGC 5838) suggesting that star-formation occurs primarily outside the centre in these two galaxies.

To conclude, extremely low values of the $[\text{O III}]/\text{H}\beta$ ratio leave no doubt that OB-stars are powering most of the nebular emission observed in the 6% of the SAURON sample galaxies (3/48), with regular dust morphologies and relaxed gas kinematics strongly suggesting that star formation could be responsible for the gas ionisation in up to 10% of the sample (5/48). The presence of young stellar populations, molecular gas, and the detection of PAHs features and strong FIR fluxes further support the case for on-going star formation in these objects. For two of them, NGC 3032 and NGC 4526, the SAURON $[\text{N I}]/\text{H}\beta$ -diagnostic diagram reveal a dramatic similarity with the star formation activity in the central rings of the early-type disk galaxies, showing also the transition to regions outside the ring where other excitation mechanisms appear to dominate, such as AGN photoionisation towards the centre. The detection in the FIRST data for NGC 3032, NGC 4526 and NGC 5838 of radio-continuum emission consistent with synchrotron radiation from relativistic electrons and free-free emission from H II-region further supports the case for on-going star-formation in these objects, whereas the non-detection of extended 1.4 GHz emission in NGC 524 and NGC 4459 can be ascribed to a lower star-formation activity and the limited sensitivity of the FIRST survey. The FIRST data also suggest that in other objects with young stellar populations and molecular reservoirs only a fraction of the $\text{H}\beta$ fluxes can be attributed to H II-regions.

3.3 Diffuse Evolved Stellar Sources

Apart from very young stars, several kinds of evolved stars or stellar remnants emit significant amounts of ionising photons, such as post-asymptotic giant branch stars (pAGB), extreme horizontal-branch stars and X-ray binaries. Although none of these objects produce an ionising continuum as powerful as that of a single O-star, their importance as photoionisation sources lies in their large numbers and potential ubiquity, in particular since early-type galaxies are made mostly of old stellar populations. In fact, the significance of pAGB stars as ionising candidates was first demonstrated by Binette et al. (1994), who showed that when taken together such objects produce a sufficient Lyman continuum to account for the $\text{H}\alpha$ luminosity of early-type galaxies. Shortly afterwards, Macchetto et al. (1996) reported the finding of a correlation (already hinted at by Phillips et al. 1986) between the $\text{H}\alpha+[\text{N II}]$ luminosity of early-type galaxies and their integrated B-band luminosity within the typical extent of the nebular emission, thus adding to the hypothesis that the principal sources of ionising photons are to be found within the bulk of the stellar population.

3.3.1 The Connection Between Nebular and Stellar Emission

Following Macchetto et al. we computed for each of our sample galaxies the average distance from the center of the detected emission-line regions, and integrated the flux of both the stellar continuum and of the $\text{H}\beta$ recombination line observed over all the SAURON spectra within such a radius. After rescaling for galactic distance, the left panel of Fig. 7 shows a nearly linear correlation between the luminosity of the $\text{H}\beta$ line and that of the stellar continuum within the average extent of the nebular emission, consistent with the narrow-band results of Macchetto et al.

Yet, the true strength of the link between the nebular and stellar emission in early-type galaxies is dramatically revealed when the total $\text{H}\beta$ luminosity is compared with the luminosity of the stellar continuum if this is integrated only *where* the nebular emission is detected. As the central panel of Fig. 7 illustrates, in this case the correlation between the values of the $\text{H}\beta$ luminosity $L_{\text{H}\beta}$ and continuum luminosity L_{cont} is much tighter¹. Such a relation is nearly, although not quite, linear (with a power-law slope $a = 1.30 \pm 0.08$), meaning that the equivalent width of the *integrated* $\text{H}\beta$ emission is almost constant across our sample. The tightness of $L_{\text{cont}}-L_{\text{H}\beta}$ relation (with a 0.15 dex scatter) is quite remarkable considering that in addition to a diffuse stellar sub-population other sources of ionisation may contribute to the total flux of the $\text{H}\beta$ recombination line. In fact, the only obvious outlier in Fig. 7 is NGC 3032, the galaxy displaying by far the most intense star-forming activity in our sample. The possible contribution of a central AGN does not affect much the $L_{\text{cont}}-L_{\text{H}\beta}$ relation, as its power-law slope and scatter do not change significantly ($a = 1.20 \pm 0.05$, 0.13 dex scatter) when the central $3''$ are excluded (§3.1). The tightness of this correlation is not a distance artifact either, since it persists also when the flux of the $\text{H}\beta$ emission and of the stellar continuum are compared (with $a = 1.31 \pm 0.08$), as shown in the right panel of Fig. 7. A direct comparison of the nebular and continuum fluxes also dispels the possibility that the observed trend is due to a sensitivity bias. As discussed in Paper V, our detection thresholds translate into a rather narrow range for the minimum equivalent width of the emission lines that we can measure, from 0.2\AA to just 0.07\AA for $\text{H}\beta$, so that in practice also the flux of barely detectable $\text{H}\beta$ lines scales with the strength of the underlying stellar continuum. Reassuringly, the right panel of Fig. 7 shows that the integrated fluxes corresponding to such detection limits not only lie comfortably below the total measured values of the $\text{H}\beta$ flux but also that they define a shallower correlation with the continuum fluxes than found in the case of the observed $\text{H}\beta$ fluxes.

The tight correlation between the integrated luminosity of the nebular emission and that of the stellar continuum stems in reality from the fact that within most of the galaxies in our sample the radial profile of the ionised-gas emission follows very closely the stellar surface brightness distribution. Figure 8 provides three specific examples (in the case of NGC 2974, NGC 3414 and NGC 4150) that vividly illustrates how well the nebular fluxes can follow the stellar continuum in early-type galaxies, or alternatively, of how the equivalent width of $\text{H}\beta$ can take remarkably similar values at very different distances from the galactic centre corresponding to very different continuum levels of the stellar surface brightness (in contrast to the case of NGC 3032, also shown in Fig. 8). In fact, across our entire sample the equivalent width of the $\text{H}\beta$ line fluctuates on average by just 32% around the mean value it takes in any given galaxy, excluding objects with obvious star formation (NGC 3032, NGC 4459, NGC 4526; §3.2) and while disregarding the central $3''$ of all galaxies to avoid any possible AGN contamination (§3.1). This is conveyed also by Fig. 9 where the $\text{H}\beta$ and continuum fluxes contributed by each bin of our sample galaxies (with the same exceptions) are plotted against each other, after rescaling the $\text{H}\beta$ and continuum fluxes observed in each galaxy to common average values. A power-law fit to such a stacked distribution indi-

¹ With the benefit of hindsight a tight correlation can also be observed in the measurements of Macchetto et al. if only the objects with diffuse and extended emission (dubbed “DE”) are considered.

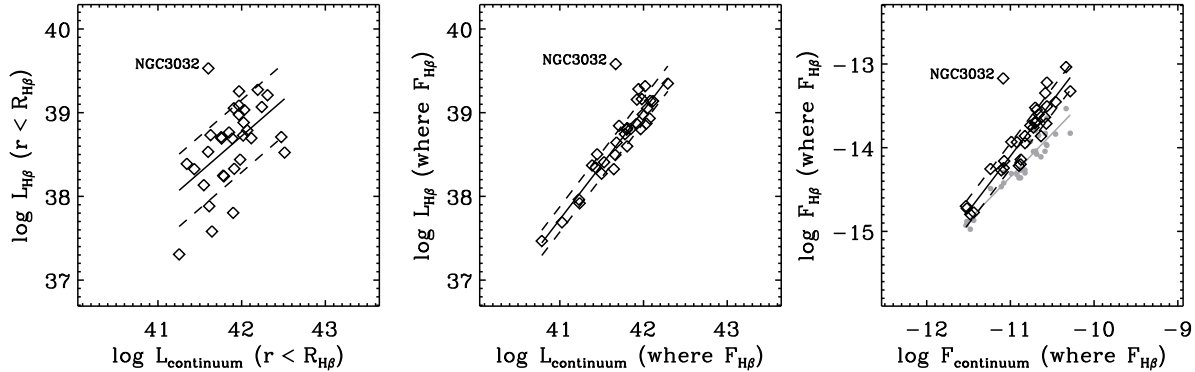


Figure 7. The connection between the integrated luminosity of the nebular emission and that of the stellar continuum in early-type galaxies. Left: Correlation between the luminosity of the stellar continuum L_{cont} and that of the $H\beta$ emission $L_{H\beta}$ observed in the SAURON spectra when both quantities are integrated within the average radius of the emission-line regions detected in each of our sample galaxies. The solid and dashed line show the best fitting power-law fit to the observed distribution and associated 1σ scatter, respectively. Middle: Same as left but now the total $H\beta$ luminosity is juxtaposed to the stellar luminosity integrated only where the nebular $H\beta$ emission is detected. A much tighter correlation persists, indicating that the $L_{\text{cont}}-L_{H\beta}$ relation is not driven by the distance distribution of our sample galaxies. The light grey points show the integrated $H\beta$ detection limits in each galaxy. Their position and alignment differs significantly from that of our integrated $H\beta$ fluxes, dispelling also any doubts that the observed correlations are due to the limited range of our equivalent width sensitivity. In all panels the position of NGC 3032, our most significant outlier, is indicated, and can be explained in terms of intense star-formation activity.

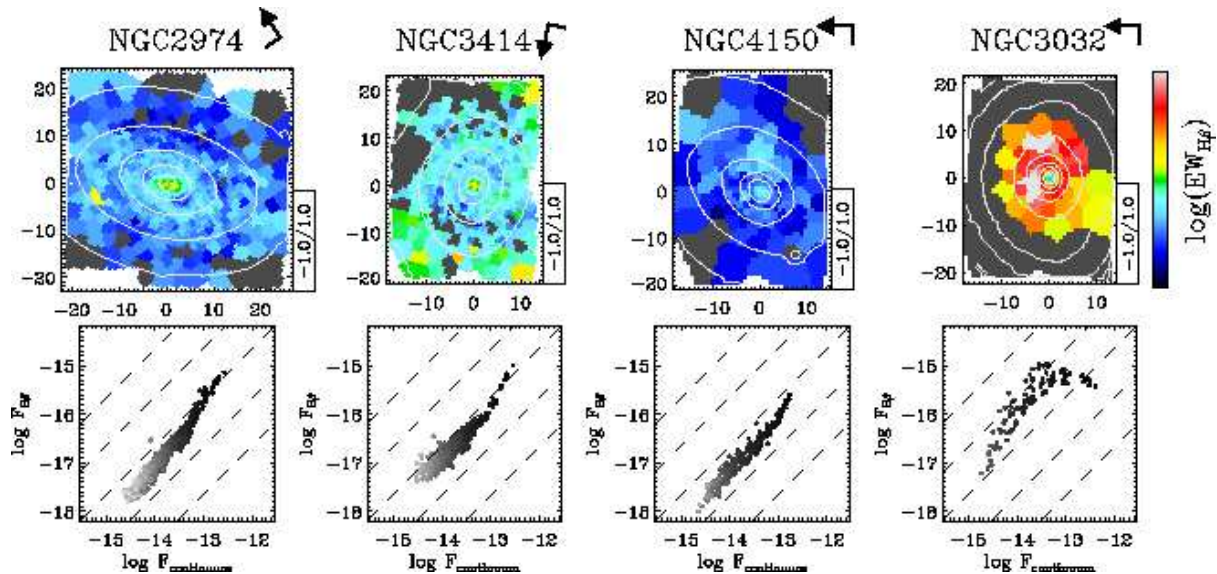


Figure 8. Examples of the local connection between the flux of the nebular emission and stellar surface brightness in early-type galaxies. Maps for the equivalent width of the $H\beta$ recombination line (*top panels*) display remarkably similar values for this quantity across most of the SAURON field of view, reflecting how closely the flux of the $H\beta$ line follows that in the stellar continuum (*lower panels*). Such a correlation breaks down in the central regions of our sample galaxies (shown with darker points in the lower panels) where AGN photoionisation can be important (§3.1), or in objects where OB-stars are the main source of ionisation (e.g. in NGC 3032, rightmost panels)

cates a nearly linear relation ($a = 0.88 \pm 0.01$) with 40% scatter (0.14 dex).

3.3.2 Explaining the Nebular to Stellar Connection

Does a nearly constant equivalent width for the recombination lines necessarily imply a diffuse stellar photoionising source? After all, the nebular flux and the stellar surface brightness, the two elements entering the equivalent width definition, relate to two different inte-

grals of the stellar luminosity density. Whereas the surface brightness is a line-of-sight integration of the luminosity density, the recombination flux is connected to the total Lyman continuum emitted by the putative ionising stellar sub-population, which reaches the gas from all directions within the galaxy.

The simplest model for the radial profile of the equivalent width of $H\beta$ can be computed in the case of a spherical galactic geometry and assuming that a constant fraction of the ionising radiation from the evolved stellar sources is absorbed and subsequently

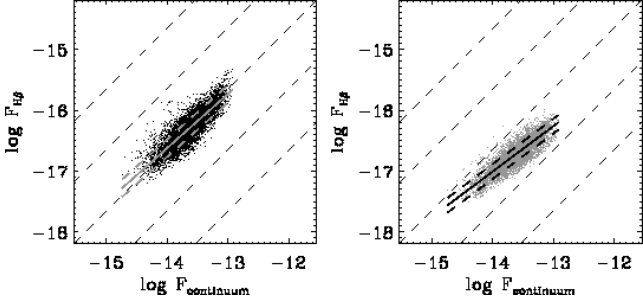


Figure 9. Correlation between the flux of the stellar continuum and the flux of the H β line (left panel) observed in each of the bin of our sample galaxies where emission is detected, except for the central 3'' and excluding the objects with obvious star formation. For each of the plotted galaxies, the continuum and nebular flux values have been rescaled to the same average value, of 2.9×10^{-14} and $6.4 \times 10^{-17} \text{ erg s}^{-1} \text{ cm}^{-2}$, respectively. The right panel shows the same correlation, but for the detection limits on the H β line, normalised by the same factor used for the observed H β values.

re-emitted across the galaxy by the ionised-gas, where the latter is also taken to reside in a planar configuration. Under the previous assumptions the equivalent width of the recombination lines at a given projected distance R from the center will be directly proportional to the ratio of total stellar radiation $F(R)$ to the stellar surface brightness $\Sigma(R)$ at the same point, since also the stellar ionising continuum reaching the gas clouds should scale with the stellar radiation $F(R)$ (for a set stellar population). For any given intrinsic luminosity density profile $L(r)$ the integral that delivers $F(R)$ is, in spherical coordinates,

$$F(R) = \int_0^\infty dr \int_0^{2\pi} d\phi \int_0^\pi \frac{L(r)}{4\pi x^2} r^2 \sin \theta d\theta \quad (1)$$

where $x = \sqrt{R^2 + r^2 - 2rR \cos \theta}$. Substituting $\cos \theta = \mu$, $d\mu = -\sin \theta d\theta$ the previous triple integral can be reduced to

$$F(R) = \int_0^\infty \frac{L(r)r^2}{2} dr \int_{-1}^1 \frac{d\mu}{R^2 + r^2 - 2Rr\mu} \quad (2)$$

$$= \int_0^\infty \ln \left(\frac{R+r}{R-r} \right)^2 \frac{r}{4R} L(r) dr \quad (3)$$

Adopting a γ -model for the intrinsic luminosity density of early-type galaxies (Dehnen 1993)

$$L(r) = \frac{(3-\gamma)M}{4\pi} \frac{a}{r^\gamma (r+a)^{4-\gamma}} \quad (4)$$

where M is the total luminosity (or stellar mass) of the galaxy and a is a scaling radius (which relates to R_e through γ), the integral given by Eq. 3 becomes

$$F(R) = \frac{(3-\gamma)Ma}{16\pi R} \int_0^\infty \frac{r^{1-\gamma}}{(r+a)^{4-\gamma}} \ln \left(\frac{R+r}{R-r} \right)^2 dr \quad (5)$$

This can be numerically evaluated by breaking it in two pieces: from $r = 0 \rightarrow R$ substituting $r = Ru$, and from $r = R \rightarrow \infty$ substituting $r = R/u$. The γ -models also allow to solve for the surface brightness profile $\Sigma(R)$ (see Appendix B of Dehnen 1993), which can be varied to include fairly shallow models ($\gamma = 1$, corresponding to Hernquist 1990 profile) as well as rather steep profiles ($\gamma = 2$, corresponding to a Jaffe 1983 profile).

With both $F(R)$ and $\Sigma(R)$ at hand, Fig. 10 shows that according to our simple model the equivalent width of the recombination lines should increase towards the outskirts of early-type galaxies,

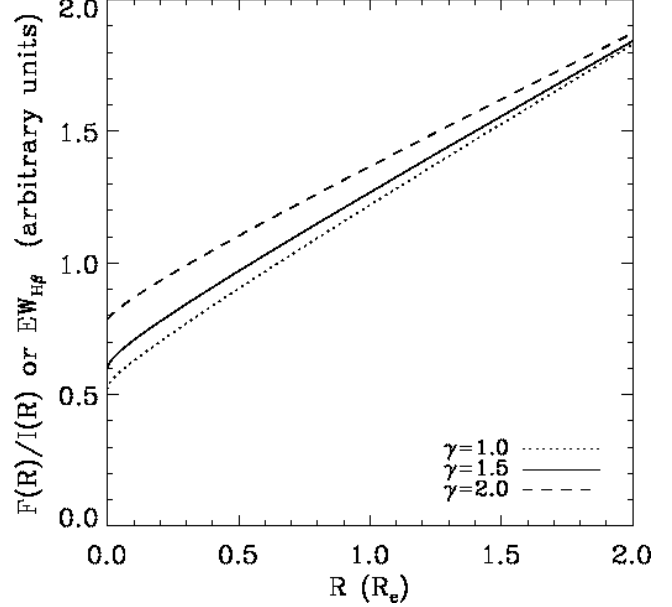


Figure 10. Predicted radial profile for ratio of the ionising radiation $F(R)$ from evolved stellar sources diffuse throughout the galaxy to the surface stellar brightness $I(R)$. Assuming that a constant fraction of $F(R)$ is reprocessed as H β emission, the plotted F/I profile provides a prediction for the radial variation for the equivalent width of H β . The model further assumes a spherical geometry and three different kind of γ -models for the intrinsic luminosity density $L(r)$, approximating a de Vaucouleurs (1948, $\gamma = 1.5$) or corresponding to Hernquist (1990, $\gamma = 1$), and Jaffe (1983, $\gamma = 2$) surface-brightness profiles. Independent of the chosen $L(r)$, the equivalent width of the recombination lines should increase towards the outskirts of early-type galaxies according to this simple model.

with little dependence on the choice of the intrinsic $L(r)$ profile. Between $\sim 10\%$ and $\sim 70\%$ of one effective radius R_e , which on average correspond to 3'' and the radius containing 90% of the emission in our sample galaxies, the model predicts a $\sim 80\%$ rise in the equivalent width of H β . Although a 0.25 dex increase may be accommodated by the average trend observed across our sample (Fig. 9), more often than not the equivalent width of the H β line tend to remain constant or even decrease with radius, in particular if we focus on the objects with the most extended and diffuse H β emission (e.g., Fig. 8) and exclude those where the impact of other sources of ionisation than evolved stars may be particularly important (e.g., the filaments of NGC 4486).

Can such a discrepancy be remedied by relaxing the simple premises of our model? An important aspect to keep in mind is that not all the ionising photons emitted by the evolved stellar sources may reach the gas due to interstellar absorption, so that only the stellar radiation emitted within the mean-free path l of the photons should be considered. This will lead to a steeper $F(R)$ profile and a shallower $F(R)/\Sigma(R)$ gradient, in better agreement with our data. Yet, as $l \rightarrow 0$ and $F(R) \rightarrow L(r) \cdot l$ the F/I ratio will eventually decrease as fast R^{-1} , again in disagreement with our observations. As regards our assumption that a constant fraction of the ionising photons is absorbed across the galaxy, this depends on how closely the radial profiles of the gas column density and of ionising radiation follow each other, and on whether the filling factor of the gas clouds varies. The column density of a steady disk increases towards the center of a realistic galactic potential well, as the models of Kawata, Cen, & Ho (2007) illustrate. The work of Kawata

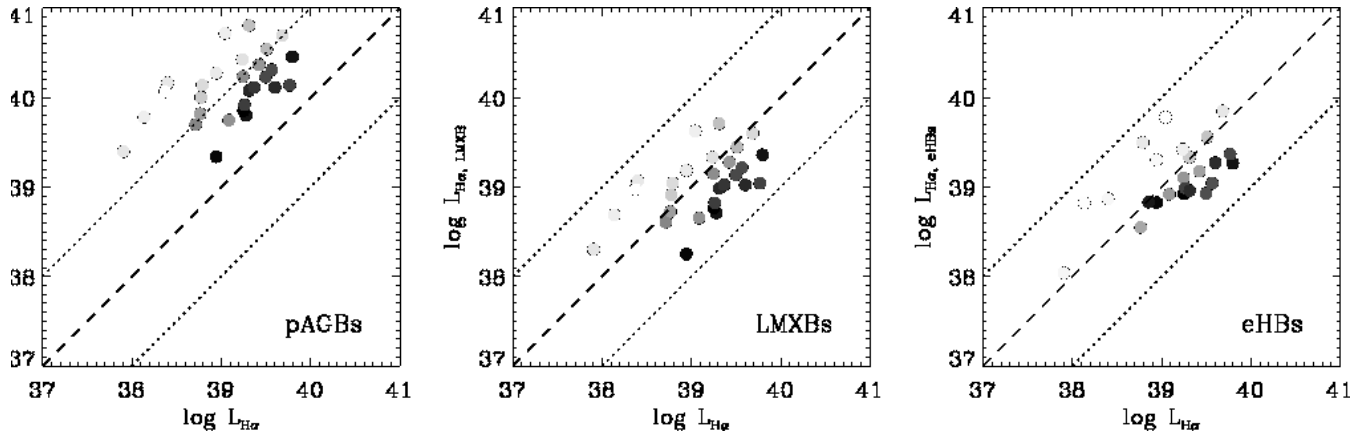


Figure 11. Ionisation balance for post-AGB stars, low-mass X-ray binaries and extreme horizontal branch stars, within the region containing 90% of the nebular emission of our sample galaxies. Darker shades of grey indicate galaxies with a higher area coverage of the ionised-gas, where the ionising flux from the stellar sources should be re-processed more efficiently. Objects where O- and B-stars have been previously established (§3.2) as the main source of ionisation (NGC 3032, NGC 4459, NGC 4526) are excluded from these diagrams.

et al. (2007) also shows that outside the very central regions the Toomre parameter Q is rather constant (see their Fig. 2), so that the gas surface density profile $I_{gas}(R)$ should scale almost exactly with the epicyclic frequency κ (given that $Q \propto \kappa/I_{gas}$). Using the γ -models to compute κ one learns that the gas surface density decreases always more gently than $F(R)$ with radius, and even more so when compared to $L(r)$. For a fixed filling factor it is therefore likely that an increasing number of ionising photons escape the galaxy as we approach the centre, whereas towards the outskirts of the gaseous disk an increasing fraction of the gas may remain neutral. The combination of a small mean-free path l and of a flattening of the $H\beta$ flux profile towards the centre (as it departs from the $F(R) \sim L(r)$ profile) could thus provide a relatively simple explanation for the general behaviour observed across our sample galaxies of a nearly constant equivalent width of $H\beta$. Alternatively, if the ionising photons travel far enough in the galaxy that $F(R)$ is not significantly affected by l , another plausible avenue to explain our data is to consider the possibility that the ionising sources are more concentrated than the bulk of the stellar populations. This may be the case if the ionising stars are also responsible for the far-UV flux ($\sim 1500\text{\AA}$) observed in early-type galaxies. The far-UV light displays indeed a steeper surface-brightness profile than observed at optical wavelengths, following closely also the metallicity gradient traced by the Mgb line-strength index (Jeong et al. 2009).

3.3.3 Ionisation Balance

In the absence of a definite model for the tight connection between the values of the stellar and nebular luminosity of early-type galaxies, we turn our attention to the energy budget. Specifically, we ask whether the various ionising stellar candidates can provide a sufficient number of ionising photons to explain the observed $H\beta$ fluxes. In doing so we return to the use of integrated flux measurements, since within large apertures the stellar luminosity estimated from the integrated flux approximates well the total luminosity within the galaxy, and therefore provides a basis for estimating the total ionising stellar radiation.

As mentioned above, Macchetto et al. (1996) already carried out the ionisation-budget exercise in the case of pAGB stars. Using

the predictions of Binette et al. (1994) for the specific ionising photon luminosity from such stars (that is, per unit mass of the entire stellar population) and assuming that all the ionising radiation is re-processed into nebular emission, Macchetto et al. could convert the stellar luminosity within the average radius of the emission-line regions into a limiting value $L_{H\alpha,pAGB}$ for the $H\alpha$ luminosity that could be possibly powered by pAGB stars. Here we revisit Macchetto et al. experiment, using the stellar population models of Yi et al. (1999) to compute the Lyman continuum from pAGB stars and 2MASS K-band images for our sample galaxies to trace the stellar mass within the radius containing 90% of the nebular emission. Consistent with previous work, the specific number of pAGB stars in the models of Yi et al. is pretty much constant between 4 and 11 Gyr, which brackets the typical age of the stellar population dominating the stellar mass of our objects. Assuming case B recombination the specific Lyman luminosity of pAGB stars in these models would deliver 0.007 erg s^{-1} in $H\alpha$ photons for each K-band erg s^{-1} , if all ionising photons are intercepted and re-processed. Under these circumstances, Figure 11 shows that pAGB stars still provide an abundant number of ionising photons to explain the ionised-gas emission observed in our sample galaxies. That the predicted limiting values $L_{H\alpha,pAGB}$ far exceed the observed values $L_{H\alpha}$ is encouraging considering that for many objects the emission-line regions cover only a fraction of the area used to compute such upper-limits (shown with a whiter shade of grey), so that almost certainly a good fraction of the pAGB ionising radiation escapes the galaxy. On the other hand, we need to keep in mind that the present stellar population models may be grossly overestimating the specific number of pAGB stars, and therefore their ability to power the ionised-gas emission in early type galaxies. The recent near- and far-UV observations of M32 with the Hubble Space Telescope by Brown et al. (2008) suggests indeed a dearth of pAGB stars compared to standard predictions for their numbers.

Turning our attention to other stellar candidates, we now consider the role low-mass X-ray binaries (LMXBs). The exquisite spatial resolution of the Chandra X-ray observatory has recently allowed to detect LMXBs in nearby ellipticals, enabling the derivation of their luminosity function and, most important in the present context, their total X-ray luminosity (in the 0.3-8 keV range; e.g. Kim & Fabbiano 2004). According to Kim & Fabbiano the LMXB

population within the optical radius of their host galaxies can deliver from a few times 10^{39} to several 10^{40} erg s^{-1} . The X-ray spectral energy distribution of LMXBs in early-type galaxies has been found to be well characterised by a simple power-law with photon index $\Gamma = 1.56$ (Irwin, Athey, & Bregman 2003), corresponding to an energy index $\alpha = 0.56$ (for $F_\nu \propto \nu^{-\alpha}$). For a power-law spectrum with an energy index $\alpha = 0.1$ to 0.9 the $\text{H}\alpha$ luminosity produced by reprocessing the X-ray emission can range from $1/9$ to $1/2$ of the X-ray luminosity (Ho 2008). Thus, to a first approximation, the overall LMXBs population of early-type galaxies could provide enough ionising photons to power the observed nebular emission, given that the $\text{H}\alpha$ luminosity of the latter ranges between a few times 10^{38} and several 10^{39} erg s^{-1} (see Paper V). Encouraged by this first check we used the relation found by Kim & Fabbiano between the K-band luminosity L_K of early-type galaxies and the X-ray luminosity $L_{X,\text{LMXBs}}$ of their LMXB population to more accurately estimate for each of our sample galaxies the limiting $\text{H}\alpha$ luminosity $L_{\text{H}\alpha,\text{LMXBs}}$ that could be powered by these stellar remnants. Upon such a closer inspection, and assuming that 18% of the LMXBs X-ray luminosity converts into $\text{H}\alpha$ emission, Fig. 11 shows that LMXBs do not live up to our expectations as ionising sources in early-type galaxies. In particular, Fig. 11 reveals that although the $L_{\text{H}\alpha,\text{LMXBs}}$ values are on average consistent with the observed $\text{H}\alpha$ luminosities, in agreement with our previous estimates, in practice none of our sample galaxies could display emission powered solely by LMXBs if the gas coverage is taken into account. In fact, in all objects with $L_{\text{H}\alpha,\text{LMXBs}} \geq L_{\text{H}\alpha}$ in Fig. 11 most the LMXBs ionising radiation is likely to escape the galaxy because of a patchy gas distribution, whereas when the gas coverage is high the LMXB population seems unable to power the nebular emission.

Finally we explore the case of extreme horizontal-branch stars (EHBs). Such low-mass core Helium burning stars only appear in significant numbers in old stellar systems, contributing in particular to the far-UV flux in populations with ages greater than 9 Gyr. For this reason, EHBs have been suggested as the dominant source for the UV-upturn observed in many early-type galaxies (e.g., Greggio & Renzini 1990) and as indicators of the oldest stellar populations (Yi et al. 1999). Although EHBs are much weaker as ionising sources than pAGB stars, their contribution to the Lyman continuum becomes nonetheless significant in stellar populations older than 10 Gyr, eventually overtaking pAGBs as the main source of ionising photons when the population turns 12 Gyr old. In order to trace the contribution of EHBs in our sample galaxies we used GALEX measurements for the far-UV flux (1341–1809Å), extracted within the area containing 90% of the nebular emission as in the case of our 2MASS measurements. Contrary to the case of the near-UV passband (centred at ~ 2310 Å), the far-UV measurements are fairly insensitive to the contribution of younger stellar components (i.e. from few 100 Myr to 1 Gyr), whereas pAGB stars do not contribute to either of these passbands. To transform the GALEX far-UV fluxes into a limiting $\text{H}\alpha$ luminosity from EHBs, $L_{\text{H}\alpha,\text{EHBs}}$, we used the models of Yi et al. to integrate the Lyman continuum due only to stars either on horizontal-branch or that have only recently evolved from it, which includes also AGB-manqué stars. We adopted models for a 11-Gyr-old stellar population, which reproduce the UV-to-optical colour observed in prototypical UV-upturn galaxies such as NGC 4552. Metallicity does not impact on our results as this parameter only produces differences in the models in UV regions (~ 1100 Å) outside the far-UV passband. In this framework the models of Yi et al. yield 0.0295 erg s^{-1} in $\text{H}\alpha$ photons for each far-UV erg s^{-1} . As in the case of LMXBs, Fig. 11

shows that EHBs per se are unlikely to generally power the nebular emission observed in early-type galaxies.

3.3.4 Summary on the Role of Evolved Stellar Sources

To conclude, we have added to early suggestions that the main source of ionisation for the gas of early-type galaxies is to be found among the bulk of their stellar population. We have found a very tight correlation between the total values of the nebular and stellar luminosity in our sample galaxies, when considering only the regions where the ionised-gas emission is detected. Furthermore, we have shown that such a global trend stems actually from the fact that the ionised-gas emission of early-type galaxies follows very closely their stellar surface brightness. Although we have not been able to conclusively explain how such a constant profile for the equivalent width of the nebular emission can be produced by stellar photoionisation, through simple modelling and reasoning we have shown the direction for future investigations without invoking embarrassing fine tuning of key parameters such as the mean free path of the ionising photons. Overall, pAGBs remain the favourite ionising candidates to explain the gas emission of early-type galaxies, which points to a need for further investigations into the present discrepancy between observations and models as regards their total numbers. The role of LMXBs would seem marginal in this context, unless future observations reveal a population of super-soft X-ray sources, which would ionise more efficiently the gas surrounding them and induce a very specific nebular spectrum (Rappaport et al. 1994). In principle, the relative importance of pAGBs, LMXBs and EHBs could be further investigated through a careful emission-line diagnostic, since this analysis can trace the specific shape of the ionising continuum of the different sources. For instance, EHBs have a much softer Lyman continuum compared to pAGBs, which should make it more difficult for EHBs to produce extended partially-ionised regions. Unfortunately a diagnostic analysis based on the [N I] emission is not possible for the diffuse component discussed here, since the [N I] lines are detected almost exclusively in the central regions of our galaxies, in the presence of star formation, or in the filamentary structures of the most massive of our sample galaxies where the interaction with the hot ISM is the most likely source of ionisation (§3.6). Notwithstanding the absence of diffuse [N I] emission, the behaviour of the [O III]/ $\text{H}\beta$ ratio is still useful in this context. Specifically, we note that strong gradients and peculiar features are *not* expected to arise easily in the presence of a uniform radiation field from the same kind of source across the galaxy, unless to consider contrived structures of higher dust concentration or enhanced gas number density that could allow for local fluctuation of the ionising parameter q . The finding of remarkable [O III]/ $\text{H}\beta$ structures suggests therefore the role of additional ionising mechanisms, such as those discussed in the next sections.

3.4 Shocks

3.4.1 Fast Shocks

Shocks offer a natural explanation for some of the most prominent and coherent structures that are observed across our sample in the maps for the equivalent width of the $\text{H}\beta$ and [O III] lines and for the [O III]/ $\text{H}\beta$ ratio, in particular for morphologies like spiral arms, oval and integral-sign shaped structures (e.g., Fig. 12). Such features can indeed be induced by the presence of stellar bars or weak triaxial perturbation of the stellar potential, which can funnel the gas into preferential streams where fast (above 100 km s^{-1}) shocks

between gas clouds may occur. Yet, the presence of equivalent-width structures per se does not guarantee that shocks are powering the gas emission - other diffuse sources (such as pAGB stars) may be still ionising the gas as this accumulates in spiral arms and similar features, where the observed emission would be stronger only due to a higher column density. On the other hand, the case for shock excitation becomes much stronger when the features in the [O III] or $H\beta$ emission are accompanied by similar structures in the [O III]/ $H\beta$ ratio. Similarly, we should expect a correlation between the strength of the recombination $H\beta$ emission and the velocity dispersion of the lines in the presence of fast shocks (see, e.g., Dopita & Sutherland 1995), because the ionising flux powered by the latter scales with the shock velocity and because unresolved velocity gradients could in principle be traced by an enhanced velocity dispersion.

Associated [O III]/ $H\beta$ structures are more often observed for integral-sign emission features (where the [O III]/ $H\beta$ distribution can be oddly asymmetric, e.g., NGC 4262, NGC 4278 and NGC 4546), and only in NGC 3414 in the case of spiral arms. As regards the gas velocity dispersion σ_{gas} , this quantity does not seem to generally trace notable equivalent-width features, except for NGC 4546 where σ_{gas} appears to display larger values along the locus of the main integral-sign structure. That remarkable equivalent-width structures are not always accompanied by similarly obvious [O III]/ $H\beta$ and σ_{gas} features (as Fig. 12 illustrates for σ_{gas}) suggests that shocks may indeed not always be the main source of ionisation in these regions. On the other hand, the shock geometry may not lead to significant broadening (as set by the spectral resolution of the SAURON data) of the emission lines along the line of sight, for instance if the shocks occur in regions that are much smaller than the physical scales that we can resolve (typically $\sim 100\text{pc}$) and if they are surrounded by a more relaxed ionised-gas medium. In this respect, it is interesting that all galaxies featuring notable spiral arms or integral-sign structures display also extended central velocity dispersion peaks (see also Fig. 12). Such central σ_{gas} gradients could mark the point where the previous limitations are overcome and the kinematic signature of the shocks can be read, if the shock fronts wind up and get closer together as the gas is funneled towards the center. This certainly appears to be the case for NGC 2974, where Emsellem, Goudfrooij, & Ferruit (2003) showed with high-resolution integral-field spectroscopic observations that the spiral-arm morphology observed in the SAURON gas maps extends well towards the centre. Emsellem et al. could also resolve better the central σ_{gas} gradient in the SAURON data, finding σ_{gas} peaks on the inner sides of the central spiral arms that further suggest the presence of shocks, although yet not necessarily that these can power the ionised-gas emission.

When [N I] emission is detected in objects with notable spiral or integral-sign features, the corresponding [N I]-diagnostic analysis is always consistent with shock-excitation. The [N I]-diagnostic is seldom conclusive, however, since most of the [N I] emission originates close to the centre of our sample galaxies (see e.g., the cases of NGC 2974 and NGC 4278 in Fig. 12) where the [N I]-diagnostic diagrams indicate that also AGN activity could be powering the gas emission. In fact, if shocks are responsible for the gas excitation in these regions, the grids of Fig. 12 suggest exceedingly high shock velocities between 300 and 500 km s^{-1} , which can hardly be explained through gravitational motions. For instance, the gas-dynamical models of Emsellem, Goudfrooij, & Ferruit (2003) for the inner regions of NGC 2974 suggest gas streamlines crossing at an angle of just 45° (see their Fig. 21), which even assuming gas motions at nearly circular speed (up to $\sim 300 \text{ km s}^{-1}$ within the

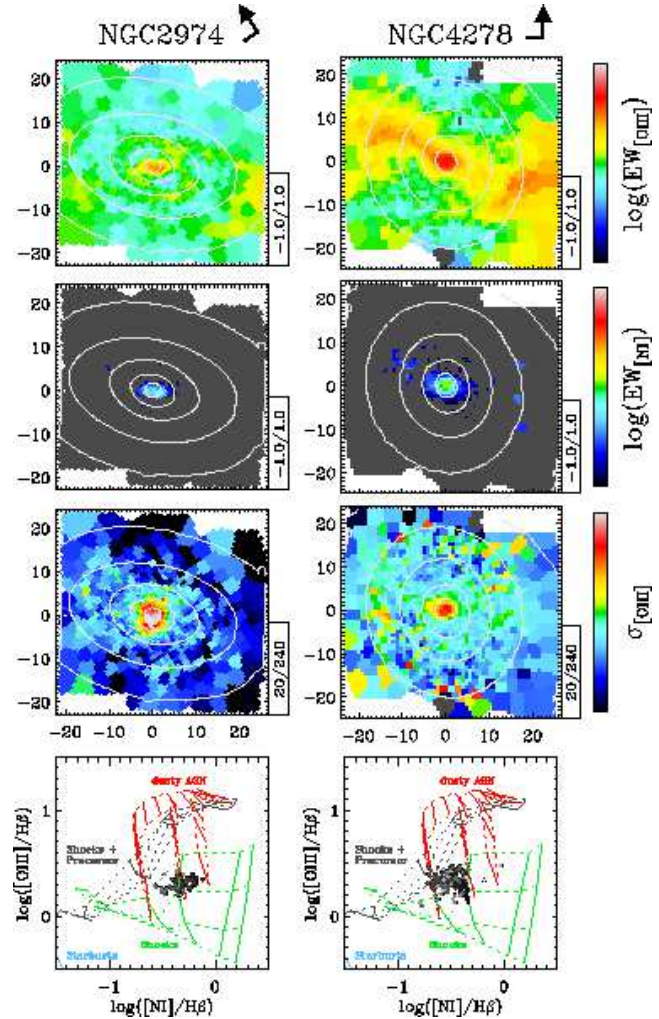


Figure 12. Two examples of elliptical galaxies where the presence of spiral-arms, ovals, or integral-sign morphologies for the ionised-gas distribution highlights the impact of non-axisymmetric perturbation of the gravitational potential on the gas motions, possibly leading to shocks between gas clouds. Emission from the [N I] doublet (second row of panels) is detected where the [O III] (upper panels) and $H\beta$ emission is the strongest, allowing for a limited emission-line diagnostic analysis (lower panels). The colored grids show the same MAPPINGS-III models as in Fig. 1, whereas the grey grids display also the predictions for shock models with a gaseous precursor ahead of the shock front. These last grids are for models with the same values of the shock velocity V_s and the magnetic parameter b as for the shock models without precursor H II regions (see the caption of Fig. 1). The [N I]/ $H\beta$ diagnostic indicates that where the [N I] lines are detected in NGC 2974 and NGC 4278 the observed emission is consistent with both AGN photoionisation and shock excitation, although in the latter case the required values for V_s would range between 300 and 500 km s^{-1} , which can hardly be attained through gravitational motions (see text). Note that increasing the electron density of the shock models ($n_e = 1$) would only shift the grid to the left as the [N I] lines collisionally de-excite more easily, which would imply even higher V_s values to power the observed emission with shocks. Maps for the gas velocity dispersion σ_{gas} (third row of panels) are also shown to illustrate how equivalent width structures (top) are not always accompanied by obvious σ_{gas} features, as expected if σ_{gas} would trace V_s .

central 2-3'' according to the models of Paper IV) would not allow to reach the required shock velocities. It thus seems unlikely that shocks are powering the nebular emission observed in the central [N I]-emitting regions of these two galaxies.

Despite the previous shortcomings shocks could still have a role in powering the gas emission observed in integral-sign features when such structures are accompanied by notable asymmetric [O III]/H β distributions, as is the case for NGC 4262, NGC 4278 and NGC 4546 (see Fig. 4 of Paper V). Excluding AGN photoionisation for such extended structures and star-formation, which usually proceed in relaxed morphologies such as rings or disks, explaining such disparate [O III]/H β values through photo-ionisation by a diffuse source such as pAGB stars would require different values for the ionising parameter q at the opposite sides of a galaxy and therefore having either different values for the gas number density or for the concentration of dust. Maintaining such different physical conditions over time would seem unlikely at first, which leaves us to consider the role of shocks. One way to explain an asymmetric distribution for the [O III]/H β ratio is to suppose that shock ionisation proceeds under different conditions ahead and behind of the shock fronts and that dust precludes us from receiving most of the nebular emission from either side of such fronts, which will naturally occur when looking at one end or the other of the galaxy. In fact, shock models such as those of Dopita & Sutherland (1995, 1996) feature the possibility of adding a gaseous precursor ahead of the shocks, which would naturally occur in gas-rich galaxies. Such precursor H II regions are characterised by high ionisation, which makes them efficient [O III] emitters and therefore good candidates as the principal source of nebular emission along the line of sight where the highest [O III]/H β values are observed. Figure 12 shows the predictions also of the shock models with a gaseous precursor, which indeed can explain the observed values for the [O III]/H β ratio that typically range between ~ 2 and 4. Yet, also in the presence of a precursor the model grids imply rather large high V_s values between 200 and 300 km s $^{-1}$, which admittedly could still be difficult to achieve, in particular in objects with well organised gas motions like NGC 4278.

In fact, our premise to discard the role of a diffuse source of ionisation in order to explain such asymmetric [O III]/H β structures, that an uneven dust distribution would be unlikely, is actually unfounded according to Spitzer observations. Based on IRAC images, in Shapiro et al. we uncover features in maps for the 8 μ m non-stellar emission excess that neatly correspond to the regions in NGC 4278 where the [O III]/H β ratio falls at its lowest value. Such a 8 μ m flux excess is usually associated across our sample to star-forming regions, and comes from ionised-PAH emission. In NGC 4278 there is no evidence for on-going star formation, however, in particular given the absence of a substantial molecular reservoir². The 8 μ m excess observed here may be due to predominantly neutral PAHs that emit more significantly in the 11.3 and 12.7 μ m bands, similarly to other early-type galaxies with PAH emission and no CO detection (see, e.g., the case of NGC 2974 in Kaneda, Onaka, & Sakon 2005). Such an asymmetric concentration of dust would induce a local hardening of the Lyman continuum from evolved stellar sources in the galaxy and would reduce the rate at which the ionising photons hit the gas clouds, thus

leading to a smaller ionising parameter q (for a discussion on dust effects see Shields & Kennicutt 1995, and references therein). Both effects would produce lower values for the [O III]/H β ratio in regions with the highest dust covering.

Finally, shocks would also spring to mind as the most likely source of ionisation for the emission observed in galaxies like NGC 3156 and NGC 3489, when glancing at the extreme range of values for the [O III]/H β ratio (from ~ 1 up to 10) that is found across the entire SAURON field of view in these objects (see Fig. 13). Yet, the high [O III]/H β values observed in these objects are inconsistent with shock excitation if we consider that NGC 3156 and NGC 3489 are among the least massive galaxies in our sample. The circular velocities in these objects peak at just ~ 150 km s $^{-1}$, which would allow only for a restricted range of shock velocities (say $V_s \leq 200$ km s $^{-1}$) and thus only for a rather limited range of values for the [O III]/H β ratio (up to 2, see Fig. 12), irrespective of the presence of a gaseous precursor. Furthermore, NGC 3156 and NGC 3489 display fairly regular gas kinematics that indicates the presence of a relaxed gaseous system, which rules out the possibility of strong non-circular motions to circumvent the previous impasse with shock excitation.

3.4.2 Slow Shocks

The dynamical deadlocks encountered in the previous subsection may suggest that slow shocks (e.g., Shull & McKee 1979), instead of fast shocks, could be important. Slow shocks could be driven by ram pressure into gas clouds as they move through the hot halo gas, and have the appealing property of producing relatively strong low-ionisation lines such as [O I] or [N I], and values of the [N I]/H β ratio close to what we observe. Even assuming that all early-type galaxies can retain a halo of hot, X-ray emitting gas, which is far from clear to be the case (e.g., Mathews & Brighenti 2003, but see also §3.6), a scenario involving slow shocks would run into two sorts of complications.

First, the values of the [O III]/H β ratio predicted by the Shull & McKee models are quite sensitive upon the shock velocity, so that in practice slow shocks would be consistent with our data only for a rather restricted range of shock velocities, between 85 and 95 km s $^{-1}$. Such a condition seems unlikely to be generally satisfied, however, considering the wide range of velocities at which the gas clouds may be orbiting within our sample galaxies.

Second, if slow shocks were generally occurring in early-type galaxies, they could lead to a profile for the equivalent width of the recombination lines that would be inconsistent with the flat profiles that we observe, and even more than what we simply estimated in the case of photoionisation by old stars (§3.3.2). If the local density of the hot gas scales like the square root of the stellar density (as in giant ellipticals, Trinchieri, Fabbiano, & Canizares 1986) we can compute the radial trend that the emission from slow shock would have, using the same simple assumptions and models of §3.3.2 and considering that the line emission from such shocks scales like the cube of the orbital velocity of the clouds (presumably close to circular) and the density of the hot halo gas. Within the same region between 10% to 90% of an effective radius that we considered in §3.3.2, the equivalent width of emission arising from slow shocks would increase markedly a factor 2.5, which is not supported by observations. Furthermore, the equivalent width of lines arising from slow shocks would drop to zero towards the centre, posing another inconsistency with the data in the absence of additional central source such as an AGN.

² The single-dish detection of Combes, Young, & Bureau (2007) in NGC 4278 is only marginal compared to other galaxies showing evidence for on-going (e.g., NGC 3032, NGC 4459 and NGC 4526) or recent (e.g., NGC 3156 and NGC 3489, see §3.5) star formation.

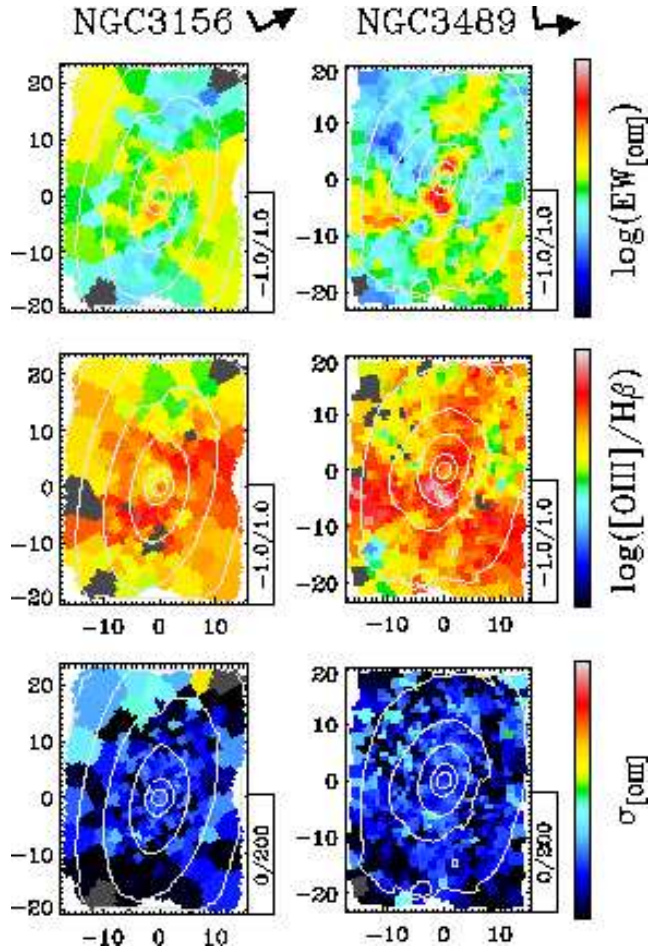


Figure 13. Two prototypical examples of early-type galaxies with intense nebular emission characterised by large fluctuations for the $[O\text{ III}]/H\beta$ ratio, which also peaks to relatively high values throughout extended regions. From top to bottom, the panels show maps for the equivalent width of the $[O\text{ III}]$ line, for the $[O\text{ III}]/H\beta$ ratio and for the gas velocity dispersion, respectively. Objects displaying such highly-ionised extended regions (HIERs) are not very massive and show invariably evidence for a recent star-formation episode. Both the intensity of the emission and the large values for the $[O\text{ III}]/H\beta$ ratio observed in HIERs can be attained considering as ionising sources the pAGB stars associated to the recently formed stellar population (see §3.5), whereas the large fluctuations in the observed $[O\text{ III}]/H\beta$ values is explained considering that star formation may still be occurring in regions with very low $[O\text{ III}]/H\beta$. The relaxed character of the gas kinematics, as traced by the extremely small values of the gas velocity dispersion, suggests that the conditions for star formation are still favourable in the specific case of these two objects.

3.4.3 Summary on the Role of Shocks

To conclude, shocks, either fast or slow, can hardly be regarded as an important source of ionisation for the diffuse nebular emission observed in early-type galaxies. In particular, we have discussed how fast shocks could contribute to power the ionised-gas emission in regions where the gas is funneled into spiral and integral-sign structures by the non-axisymmetric perturbations of the gravitational potential. Yet, even there the role of diffuse stellar sources may be as, if not more, important than shocks, in particular when the spiral and integral-sign features in maps for the $[O\text{ III}]$ or $H\beta$ emission are not accompanied by similar $[O\text{ III}]/H\beta$ structures. In the central regions of our sample galaxies shocks could contribute

to explain the high values for the gas velocity dispersion, but limited $[N\text{ I}]$ diagnostic analysis combined with simple dynamical arguments appear to dismiss shocks as the main source of gas excitation. Arguments for the importance of shocks, which included also the presence of a gaseous precursor and of dust, were put forward also to explain the peculiar asymmetric $[O\text{ III}]/H\beta$ distribution that is often associated to integral-sign emission structures, but ultimately run into a similar dynamical dead lock. In these cases Spitzer observations reveal an uneven distribution of dust, which can help reconcile the observed $[O\text{ III}]/H\beta$ character of the nebular emission with simple photoionisation by diffuse stellar sources. Finally, we have also considered the case for shock excitation in low-mass galaxies with high-ionisation extended regions, and eventually ruled out shocks as the main source of ionisation. In the next section we will consider an alternative explanation for such extreme cases.

3.5 Post Starbursts and High-Ionisation Extended Regions

An intriguing subset of the early-type galaxies surveyed in the course of the SAURON survey consists of relatively small objects (with $\sigma_e \leq 120\text{ km s}^{-1}$) displaying high-ionisation extended regions (HIERs), where the $[O\text{ III}]/H\beta$ ratio reaches some of the most extreme values observed in our sample with great variations across the SAURON field of view (Fig. 13). NGC 3156 and NGC 3489, which we already considered in §3.2 and §3.4, represent only the most remarkable examples of such a kind of early-type galaxies - HIERs are also found in NGC 7332 and NGC 7457 (see Fig 4 of Paper V). A common trait that these low-mass objects share is the presence throughout the galaxy of fairly strong $H\beta$ absorption features (Paper VI), which is indicative of a recent star-formation episode. In fact, star formation in NGC 3156 and NGC 3489 may have not yet come to a complete halt, in particular in those relatively small regions where very low values of the $[O\text{ III}]/H\beta$ ratio are observed. Both PAH and CO reservoirs have been detected in these galaxies (see Shapiro et al. 2009 and Combes, Young, & Bureau 2007, respectively), although the amount of molecular material found in NGC 3156 and NGC 3489 ($M_{H_2} = 0.2, 0.1 \times 10^8 M_\odot$) is significantly less than what found in the presently star-forming galaxies NGC 3032, NGC 4459 and NGC 4526 (with $M_{H_2} = 2.5, 1.7, 3.7 \times 10^8 M_\odot$). Additionally, the gas kinematics in NGC 3156 and NGC 3489 trace a remarkably cold dynamical system (the values of the gas velocity dispersion σ_{gas} observed in NGC 3156 and NGC 3489 among the smallest measured in our sample, $\sim 50\text{ km s}^{-1}$) which could still favour the formation of stars. All these facts suggest that these objects are post-starbursting systems, perhaps linked to “E+A” galaxies³ (Dressler & Gunn 1983).

Is the high-ionisation character of the nebular emission from these objects linked to their recent star-formation history? In the context of AGN activity, Taniguchi, Shioya, & Murayama (2000) considered the role of post-starbursting stellar systems to explain the LINER and Seyfert emission of nearby galactic nuclei. Namely, Taniguchi et al. recognised that as the most massive and recently formed stars start leaving the asymptotic giant branch ($\sim 10^8$ yrs after the starburst), the corresponding planetary nebulae nuclei become an important and sufficiently hot source of ionising photons.

³ The very nuclear regions, within the few tens of pc, of NGC 3489 already display the classical features of an E+A spectrum (Sarzi et al. 2005).

Whereas this scenario is fairly limited in explaining AGNs, in particular since most galactic nuclei are invariably old (e.g., Sarzi et al. 2005, but see also Ho 2008), photo-ionisation from the pAGB population associated to a recent starburst is a very likely ionising mechanism for the HIER emission observed in low-mass early-type galaxies.

According to Taniguchi et al., to power with pAGB stars from massive progenitors (between 3 to 6 M_{\odot}) the $H\alpha$ luminosity of NGC 3156 and NGC 3489, which is around $\sim 10^{39}$ erg s $^{-1}$, these objects should have experienced a starburst involving approximately $\sim 10^9 M_{\odot}$ of gas, this is consistent with our estimates for the amount of stars that should have recently formed in these galaxies (corresponding to 10% of the total mass) in order for the values of their stellar and dynamical mass-to-light ratio to agree with each other as is the case for more quiescent early-type galaxies in the SAURON sample (Paper IV).

Another attractive feature of such a post-starburst photo-ionisation scenario is that it could naturally account for the extreme values of the [O III]/ $H\beta$ ratio observed in early-type galaxies with HIERs. The pAGB population associated with the recent starburst is presumably still confined to the galactic plane where star formation took place and where the remaining gas is still orbiting, thus bringing the gas much closer to its photoionising sources than is the case for the pAGB stars related to the older bulge population (§3.3). In turn this situation would translate into an higher ionisation parameter q and therefore to larger values for the [O III]/ $H\beta$ ratio. We note also that due to their proximity to the gas, the Lyman continuum of the pAGB stars associated to a recent starburst could be reprocessed as nebular emission more efficiently than for other stellar sources throughout the bulge. This would help explaining also the remarkable strength of the nebular emission in objects like NGC 3156 and NGC 3489, where the equivalent width for the integrated $H\beta$ and [O III] lines reaches values of 0.5Å and 1.5Å, respectively.

To conclude, in approximately 10% of the early-type galaxies in the SAURON sample the nebular emission is most likely powered by pAGB stars associated to a recently formed population of stars. The intense and highly-ionised character of the observed emission in these objects can be explained by the vicinity of the gas to its ionising stellar sources, which are presumably still confined to the galactic plane where they formed. The nature of the nebular activity observed in the post-starbursting systems of the SAURON sample could also have bearings for our understanding of the “E+A” phenomenon. “E+A” galaxies are extremely rare objects (e.g., Kaviraj et al. 2007) that display strong Balmer absorption lines but no nebular emission, suggestive of a recent but already exhausted, perhaps even quenched, star-formation episode. Yet, “E+A” are not totally devoid of gas since they often still display abundant H I reservoirs (Buyle et al. 2006), which, according to our picture, could be re-ionised just a few $\sim 10^8$ yrs after the starburst. This would leave only a very short time after the death of OB-stars for the galaxy to appear quiescent while developing A-star type features, which could contribute to explain why so few post-starbursting galaxies are observed in their “E+A” phase.

3.6 Interaction with the Hot Interstellar Medium

Historically, it was perhaps the finding of optical emission in and around the most massive galaxies of X-ray selected clusters that first drew considerable attention to the ionised-gas component of early-type galaxies (Hu, Cowie, & Wang 1985; Heckman et al.

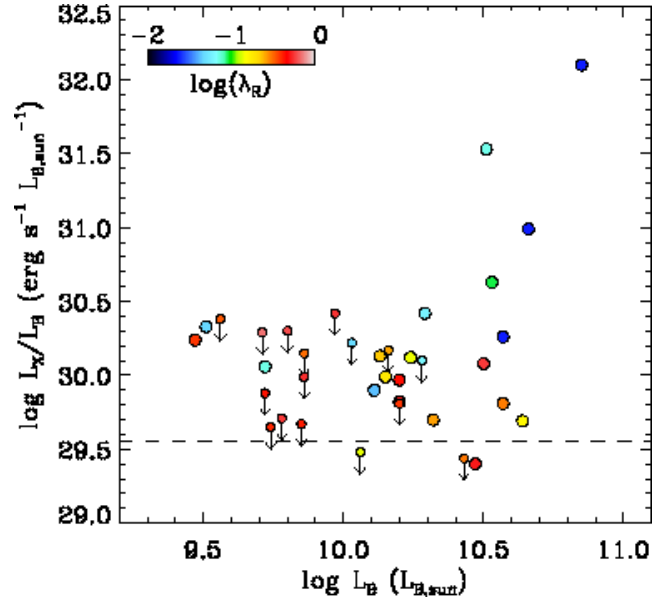


Figure 14. X-ray properties of SAURON early-type galaxies. The total blue-band luminosity L_B is compared to the X-ray luminosity L_X , normalised to L_B . Symbols are colour-coded according to the observed degree of rotational support as traced by the λ_R parameter of Emsellem et al. (2007), with green or blue symbols showing slowly- or non-rotating objects with $\lambda_R < 0.1$. L_X values (circles) or upper limits (small circles with downward arrows) are ROSAT and Einstein measurements from the compilation of O’Sullivan, Forbes, & Ponman (2001), except for NGC524 and NGC5813, which were taken from Pellegrini (2005) and Böhringer et al. (2000), respectively. These data cover three-quarters of the SAURON early-type sample, with the remaining objects being typically low-luminosity galaxies with an average $\log L_B \sim 9.9$. The horizontal dashed line shows the normalised X-ray luminosity expected from stellar sources (O’Sullivan, Forbes, & Ponman 2001). Only luminous galaxies can retain massive X-ray halos, in particular if they are slowly- or non-rotating objects.

1989). The discovery of such a warm medium was indeed regarded as a major success of the cooling flow theory (Fabian 1994), although it soon became apparent that the amount of ionised gas found in the optical filaments of X-ray clusters exceeded by far the rates predicted by cooling flows (Heckman et al. 1989). Furthermore, the presence of dust in such filaments posed an additional problem to the cooling flow scenario since gas cooling down from a KeV plasma should not be dusty and since dust particles ought to be quickly destroyed by X-ray sputtering in environments permeated by hot ions (e.g., Donahue & Voit 1993). The connection between the X-ray and optical emission in and around the most massive early-type galaxies remained an established fact, however, which led to the suggestion that the nebular emission arises in fact from material that has been recently accreted and that is being excited by the hot medium itself, either through thermal electron conduction (Sparks, Macchetto, & Golombek 1989; de Jong et al. 1990) or by the radiation that the hot gas emits as it cools down (Voit & Donahue 1990). Sparks et al. (1989) showed that the energy flux provided from heat conduction is sufficient to explain the nebular emission, whereas Donahue & Voit (1991) found that the X-ray gas radiation could explain also the typical line ratios observed in the optical filaments of cooling flows clusters (see also Ferland et al. 2009, for a recent investigation). Yet, the most spectacular confirmation of the connection between the hot and

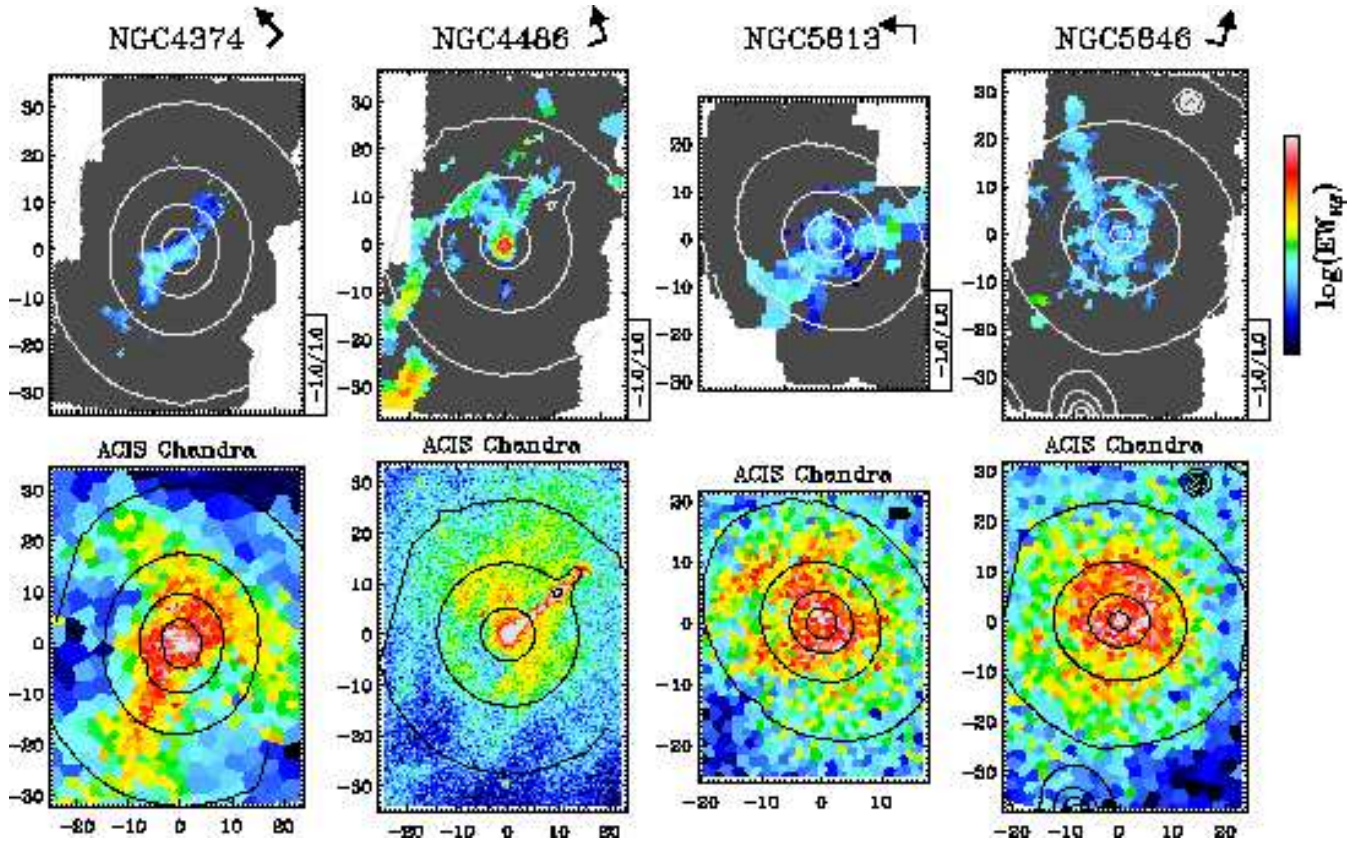


Figure 15. Warm *versus* hot gas emission in the four brightest and slowly- or non-rotating galaxies in the SAURON galaxies, which all show also prominent dust lanes. The top panels show SAURON maps for the equivalent width of the $H\beta$ line, in \AA and on a logarithmic scale, whereas the lower panels show Voronoi-binned maps for the X-ray emission observed with Chandra, in the 0.3–5.0 keV band. Except for only a few regions, the nebular emission is generally associated to X-ray emitting features. For NGC 4486 and NGC 5846, this connection was already discussed by Sparks et al. (2004) and Trinchieri & Goudfrooij (2002), respectively.

warm phases of the ISM came when X-ray images of high spatial resolution revealed a striking spatial coincidence between regions displaying optical and X-ray emission, first in the case of M87 (Young, Wilson, & Mundell 2002; Sparks et al. 2004) and then in NGC 5846 (Trinchieri & Goudfrooij 2002).

In light of these findings we turn our attention to the interaction between the warm and hot phases of the ISM, as the last ionising mechanism that we will consider in order to explain the nebular emission observed across our own sample of early-type galaxies. Unsurprisingly, it is only the most luminous galaxies in the SAURON sample that can retain a massive halo of hot, X-ray emitting gas, although the degree of rotational support also appears to play a part in determining the presence of an X-ray atmosphere. Figure 14 vividly illustrates this point by showing how only the brightest galaxies feature values of the X-ray luminosity (mostly from the compilation of O’Sullivan, Forbes, & Ponman 2001) that well exceed what is expected from an unresolved population of LMXBs, in particular if considering slowly- or non-rotating galaxies (green or blue circles). All but two (NGC 4552, NGC 5982) of such massive systems display prominent dust features (see the HST maps of Paper V), and luckily Chandra images are available for these dusty giant galaxies (NGC 4374, NGC 4486, NGC 5813, NGC 5846) in order for us to investigate the connection between the X-ray and optical emission.

Figure 15 compares the Chandra X-ray images for the four

brightest slowly- or non-rotating galaxies in the SAURON sample with maps for their $H\beta$ emission from Paper V. The Chandra images show integrated fluxes in the 0.3 – 5.0 keV energy band and have been spatially rebinned through Voronoi tessellations (Cappellari & Copin 2003) to reach a minimum of 10 counts per bin. Except in only a few regions, the ionised-gas emission is usually associated to X-ray emitting features, whereas the converse does not always hold. Thus, with NGC 4374 and NGC 5813 we bring two additional examples besides NGC 4486 and NGC 5846 of objects displaying such a remarkable coincidence between the hot and warm phases of the ISM. Sparks et al. (2004) could also show that the X-ray filaments of NGC 4486 have a lower temperature than the surrounding medium, supporting the idea that heat is being transferred from the hot to the warm gas. Unfortunately the Chandra images for the other objects in Fig. 15 are not sufficiently deep to allow the same kind of analysis, since binning up to reach the minimum signal quality for a sensible spectral analysis (usually 50 counts) would leave only a few patches. Yet, our integral-field data reveal another characteristic of the ionised-gas emission in such dusty giant slowly- or non-rotating galaxies that sets them aside from the rest of the SAURON sample and which reinforces the case for gas excitation through the interaction with the hot medium.

Figure 16 shows indeed how the optical filaments of such dusty giant ellipticals display rather intermediate values for

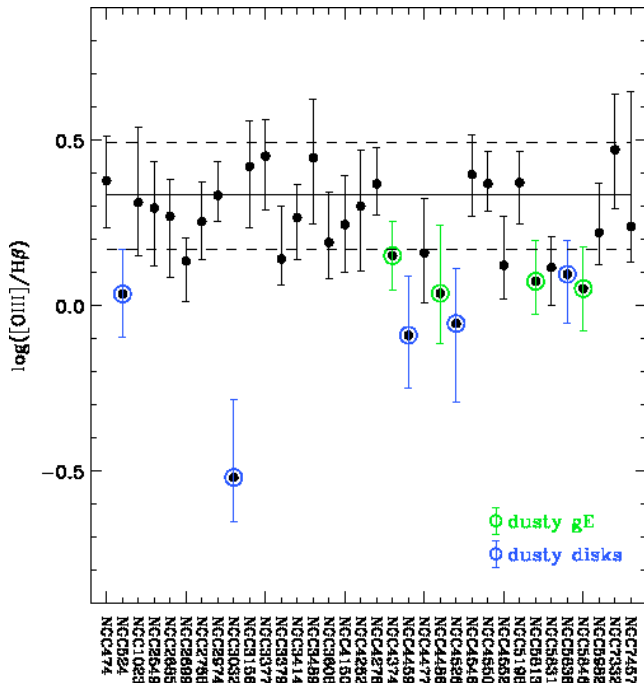


Figure 16. Median values and 1σ confidence limits for the $[\text{O III}]/\text{H}\beta$ ratio observed in the SAURON galaxies with clearly detected and extended $\text{H}\beta$ and $[\text{O III}]$ emission, plotted in alphabetical order against the galaxy name. The brightest, dusty and slowly- or non-rotating ellipticals are shown with green symbols, objects with dusty disks and on-going star formation are shown in blue, and the remainder of this subsample is denoted in black. The horizontal dotted and dashed lines show the average and 1σ boundary for the $[\text{O III}]/\text{H}\beta$ ratios observed in the galaxies shown by the black points. The tendency for the dusty giant ellipticals to show lower values for $[\text{O III}]/\text{H}\beta$ ratio than for the rest of the quiescent galaxies in the SAURON sample suggests, in light of the presence in these objects of a massive halo of X-ray emitting gas, that the interaction between the hot and warm phases of the ISM has an impact on the ionisation of the nebular plasma.

the $[\text{O III}]/\text{H}\beta$ ratio ($\sim 1-1.5$), which lie below the average $[\text{O III}]/\text{H}\beta$ values observed in the other quiescent early-type galaxies in the SAURON sample. This low-ionisation pattern is reminiscent of the low $[\text{O III}]/\text{H}\beta$ values that are observed in the optical filaments in and around the brightest cluster galaxies (e.g. Sabra, Shields, & Filippenko 2000; Hatch et al. 2006). Yet, in such environments the $[\text{O III}]/\text{H}\beta$ ratio falls to much lower values than we observe in our sample galaxies when optical and X-ray emission coincide. For instance, Hatch et al. (2006) hardly detect any $[\text{O III}]$ emission in the filaments that extend well beyond the optical boundaries of NGC1275, the brightest member of the Perseus cluster, whereas in the inner region of the same ionised-gas nebula Sabra, Shields, & Filippenko (2000) measure $[\text{O III}]/\text{H}\beta \sim 0.3-1$, still below the values that we find in the four galaxies of Fig 15. Rather than considering varying Oxygen abundances, Hatch et al. interpret this behaviour as an ionisation gradient driven by a progressive intensification of the excitation mechanism toward the optical regions of NGC1275. We agree with this conclusion, and further suggest that the intermediate $[\text{O III}]/\text{H}\beta$ values observed in the optical regions of our sample galaxies where hot and warm gas appear to interact are in fact caused by the contribution of stellar photoionisation, in addition to the interaction with the hot ISM. There is indeed no reason to exclude in dusty giant ellipticals the presence of a Lyman continuum from old stars, which per se would

lead to the larger $[\text{O III}]/\text{H}\beta$ values that are observed in the rest of the quiescent early-type galaxies of the SAURON sample. In fact, we note that for the optical filaments associated to X-ray features the radial profile of the $\text{H}\beta$ flux tends to follow rather closely the stellar surface brightness, further suggesting the importance of stellar photoionisation.

To conclude, in the brightest and slowly- or non-rotating early-type galaxies the presence of a massive halo of hot, X-ray emitting gas imprints a distinct low-ionisation character to the emission-line regions beyond the direct influence of a central AGN. This line-ratio pattern is achieved thanks to the energy input provided by the hot gas as it interacts, presumably through heat conduction, with the warm gas, which is still subject to photoionisation from old stellar sources like in other early-type galaxies. As reported in previous work, also in the dusty giant galaxies of the SAURON sample a remarkable spatial coincidence between optical and X-ray emitting features testify to the interaction between the hot and warm phases of the ISM.

4 IMPLICATIONS FOR LARGE-SCALE SURVEYS

If the high sensitivity of the SAURON survey has revealed the extent to which diffuse ionised-gas emission is found in nearby early-type galaxies (up to $\sim 75\%$, Paper V), shallower but much larger spectroscopic campaigns such as the Sloan Digital Sky Survey (SDSS) can help reveal through shear numbers important connections between the nebular and stellar properties of early-type galaxies (e.g., Kauffmann et al. 2003; Graves et al. 2007; Schawinski et al. 2007; Kewley et al. 2006; Kauffmann & Heckman 2009). The nebular activity detected in the SDSS spectra of early-type galaxies is, according to standard BPT-diagnostics (see also §2), generally either LINER-like or characterised by composite H II/Seyfert-like emission (often referred to as transition objects, or TOs), especially when early-type galaxies are selected on the basis of their red colour rather than by their morphology (Schawinski et al. 2007). Such a kind of nebular emission is most often taken as due to a central AGN (e.g., Kauffmann et al. 2003; Kauffmann & Heckman 2009; Kewley et al. 2006), although unlike for H II and Seyfert nuclei there are a number of plausible ionising mechanisms that can power composite and LINER-like emission. This is particularly relevant if one considers that the fixed $3''$ -wide aperture of the SDSS spectra usually encompasses large Kpc-scale regions where diffuse emission such as that observed across our sample could contribute to the SDSS nebular fluxes. In fact, other sources than a central AGN may significantly contribute to power the central LINER-like emission of even much closer galaxies, and therefore over much smaller physical regions than in the case of SDSS spectra, typically on 100 pc scales (see, e.g., the case of the Palomar survey, Ho 2008).

We can use our previous results on the relative importance of the various ionising mechanisms at work in and across different kinds of early-type galaxies in order to better understand the nature of the nebular emission observed in early-type galaxies in large-scale surveys, addressing in particular the real extent of AGN activity. Indeed, we can exploit the integral-field nature of the SAURON data to simulate how our sample galaxies would appear if observed through wide circular apertures, as is the case for distant early-type galaxies targeted by the SDSS. A good starting point for such a comparison between SAURON and SDSS data is the MoSES sample of Schawinski et al. (2007), which includes morphologically se-

lected early-type galaxies with redshift values between $z = 0.05$ and $z = 0.1$. Using the SDSS pipeline parameter `devRad_r` as a proxy for the effective radius R_e , in 68% of the MoSES objects the $3''$ -wide aperture of the SDSS spectra encompasses between 32% and 79% of R_e , an area which is almost always covered by the SAURON observations of our local sample. At these galactic scales, nebular emission is detected in the MoSES sample in 18.5% of the cases, with values for the equivalent width of the [O III] emission typically (68%) between 0.8\AA and 4.3\AA , extending most often to 2.9\AA and 2.4\AA if we consider only objects with composite or LINER-like emission, respectively. Seyfert nuclei and star-forming objects indeed make up the majority of the MoSES galaxies with the most intense emission.

Figure 17 shows the radial profiles for the integrated flux and equivalent width of the [O III] emission over increasingly large circular apertures, for the 9 SAURON galaxies that display sufficiently intense emission to be detected at the typical sensitivity of the MoSES spectra. Out of these 9 objects one is a star-forming galaxy (NGC 3032) whereas the remaining 8 show integrated values of the [O III]/H β ratio in the $\log([\text{O III}]/\text{H}\beta) = 0 - 0.5$ range, which is typical of LINER-like emission (e.g., Ho et al. 1997, TOs can extend to lower [O III]/H β values). These 8 SAURON galaxies cover fairly well the range of equivalent width values observed for most of the MoSES objects with composite and LINER-like emission (in particular the latter), but fail to extend in the most intense regime occupied more often by MoSES Seyfert nuclei and strongly starbursting galaxies. To some extent this is to be expected considering that Seyfert nuclei are exceedingly rare, making up only 1.5% of the MoSES sample, and given that H II-nuclei are most often found in low-mass early-type galaxies, which are particularly under-represented in the SAURON sample since this is a representative but incomplete sample of the nearby early-type population (de Zeeuw et al. 2002). Yet, this may also suggest that the most intense regime of emission is where truly nuclear LINER and composite activity can be found in SDSS spectra. In fact, of the SAURON galaxies with detectable LINER-like emission at the MoSES sensitivity level only half show radio or X-ray signposts of AGN activity (§3.1). Furthermore, even in these cases the normalised profiles for the integrated flux of the [O III] emission (Fig. 17, top panel) illustrate how the regions dominated by AGN activity (within $3''$, according to the conservative estimates of §3.1) would contribute at most between 30% and 55% of the total [O III] emission detected within the MoSES apertures. Thus the SAURON galaxies that, if placed at the distance of the MoSES galaxies, would display the typical values for the equivalent width of [O III] and for the [O III]/H β ratio of the MoSES LINER-like galaxies are in fact mostly, if not completely, dominated by diffuse emission powered by other sources other than a central AGN, most likely post-AGB stars (§3.3).

At first glance, the fraction of SAURON objects (9 out of 48, or $19 \pm 6\%$) with detectable integrated emission at the MoSES sensitivity level (hereafter referred simply as “detectable”) would also seem consistent with the fraction of the MoSES sample displaying nebular emission (18.5%), even when the fraction of star-forming systems (1 out of 48, or $2 \pm 2\%$ compared to 4.3%) or of galaxies with composite or LINER-like emission (8 out of 48, or $17 \pm 5\%$ compared to 12.6%) are considered separately. Yet, it should be noted that the objects with composite emission in the MoSES sample come typically (68%) with $\log([\text{O III}]/\text{H}\beta)$ values between -0.25 and 0.28 , whereas the 8 “detectable” and non-starforming SAURON galaxies show $\log([\text{O III}]/\text{H}\beta)$ values between 0.29 and 0.43 , a range that is much closer to that of the MoSES galaxies with LINER-like emis-

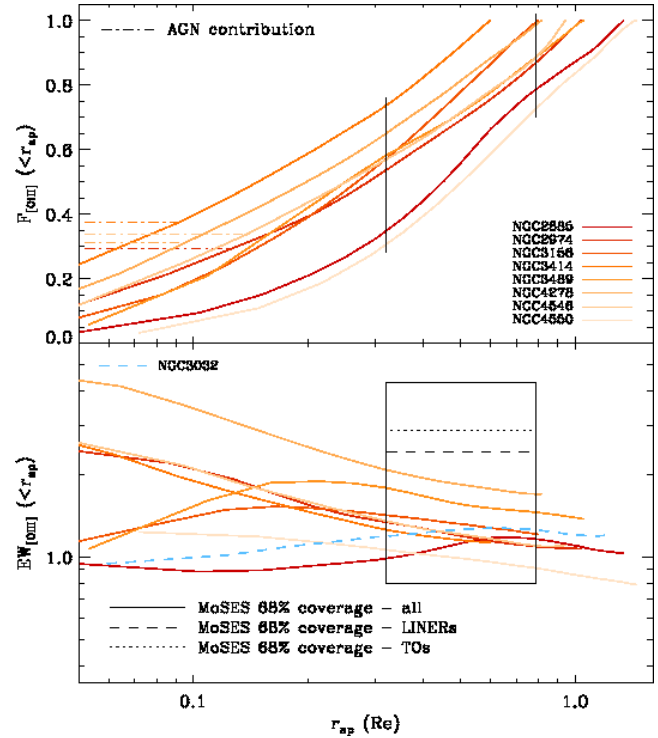


Figure 17. Radial profiles for the integrated flux (normalised to the total, top panel) and equivalent width of the [O III] $\lambda 5007$ emission (lower panel) for the SAURON galaxies that display sufficiently intense emission to be detected at the typical sensitivity of the SDSS spectra for the MoSES early-type galaxy sample of Schawinski et al. (2007). The integrated flux and equivalent width values are obtained over circular apertures with radii expressed in units of the galaxy effective radius R_e . In the lower panel, the rectangle drawn with solid lines indicates where 68% of the values for the physical size of the galactic regions that are encompassed by the $3''$ -wide aperture of the SDSS spectra are located, while also showing where 68% of the values for the equivalent width of the [O III] emission detected in the MoSES spectra can be found. In the same rectangle, the dotted and dashed horizontal lines show the upper extent of the region containing 68% of the values for the equivalent width of the [O III] emission observed only in the MoSES galaxies displaying composite and LINER-like emission, respectively. In the upper panel, the dot-dashed horizontal lines show, for the galaxies with Radio or X-ray signposts of nuclear activity, the most conservative contribution of the AGN to the total [O III] flux (that is, within $3''$; see §3.1), whereas the vertical lines show again the typical size of the galactic regions observed by the MoSES spectra, which can be used to estimate the AGN contribution to the nebular emission measured in such SDSS data.

sion (where $\log([\text{O III}]/\text{H}\beta)$ spans between 0.18 and 0.55). To put it in a more direct way, the fraction of the MoSES sample that displays $\log([\text{O III}]/\text{H}\beta)$ values in the $0 - 0.5$ range, which is generally associated with LINER-like emission, is just 8.3%, or only about half the fraction of the “detectable” SAURON galaxies with integrated $\log([\text{O III}]/\text{H}\beta)$ values in the same range. It is possible that the lack of “detectable” SAURON galaxies with integrated values for [O III]/H β ratio that are more typical of composite activity is due to small-number statistics and the incomplete character of the SAURON sample. Indeed, as for the objects displaying star formation and Seyfert activity, also the MoSES galaxies with composite emission live preferentially in low mass early-type galaxies, which are particularly under-represented in the SAURON sample. Alternatively, it is possible that some of the MoSES galaxies would not be classified as early-type if observed at a much closer distance. At

least for a local point of view, a more quantitative analysis will have to wait for a complete integral-field survey of the nearby early-type galaxy population, which will be possible once the data from the ATLAS^{3D} campaign⁴ are at hand.

Notwithstanding the limitations of the present analysis, the picture we have drawn for SDSS galaxies with [O III]/H β ratios typical of LINER-like emission (of which we have an overabundance of “detectable” SAURON examples) would reinforce the recent results of Stasińska et al. (2008), who advocate the importance of photo-ionisation by post-AGB stars in “retired” galaxies to explain the LINER population in the SDSS survey. Yet, we note here that 2 out of the 8 “detectable” SAURON objects with LINER-like values of the [O III]/H β ratio are most likely powered by post-AGB associated to a recent star-formation episode (NGC 3156 and NGC 3489, §3.5) rather than to the older bulge population. This kind of sources could be particularly common in the SDSS LINER population, considering that such SAURON post-starbursting systems appear to be more easily “detectable” in SDSS spectra (50%, or 2 out of 4) than is the case of the other SAURON galaxies with diffuse LINER-like emission but uniformly old stellar populations (25%, or 6 out of 25). In fact, such a post-starburst LINER-like activity could contribute to explain the findings of Graves et al. (2007), that red-sequence SDSS galaxies with strong LINER-like emission show younger stellar populations, in particular in less-massive systems, such as NGC 3156 and NGC 3489.

To conclude, our SAURON integral-field data suggest that in very few, if any, of the SDSS galaxies which display only modest values for the equivalent width of the [O III] line (less than $\sim 2.4\text{\AA}$) and LINER-like values for the [O III]/H β ratio, the nebular emission is truly powered by AGN activity. Only the most intense, and rarer, manifestations of LINER nuclear activity can be detected against both the stellar background encompassed by the SDSS aperture and the diffuse emission observed in early-type galaxies, unless to consider a very small minority of the closest SDSS objects. For SDSS samples that share these equivalent-width and line-ratio characteristics, the [O III] $\lambda 5007$ line is thus problematic as a diagnostic of low levels of black-hole growth, and LINERs may represent a mixed population that does not uniformly trace low-Eddington ratio accretion.

5 CONCLUSIONS

Building on our previous investigation of the incidence, morphology and kinematics of the ionised gas in the early-type galaxies of the SAURON sample, in this paper we set out to address the question of what is powering the nebular emission observed in them.

To constrain the possible sources of gas excitation we resorted to a variety of ancillary data ranging from radio to X-ray wavelengths, drew from complementary information on the gas kinematics, stellar populations and galactic potential from our SAURON data, and introduced a SAURON-specific diagnostic diagram based on the [N I]/H β line ratio as a gauge for the hardness of the ionising continuum. Using SDSS data for galaxies with strong emission we have shown that the [O III]/H β vs [N I]/H β diagram is a powerful tool to isolate star-forming regions and to clearly separate Seyfert and LINER nuclear activity. To best use the [N I]/H β

diagnostic we re-extracted more reliable [N I] measurements from the SAURON data using a new array of model and empirical templates based on the MILES stellar library. Such empirical templates come from fits to high-quality SAURON spectra extracted over regions in most cases devoid of emission lines and with values for the absorption-line strengths that cover well the range observed across our sample.

The considerable range of values for the [O III]/H β line ratio found both across the SAURON sample and within single galaxies has prompted us to explore the relative importance of a central AGN, star formation, old UV-bright stars, shocks and of the interaction with the hot phase of the ISM in powering the nebular emission from early-type galaxies. The role of these ionisation sources can be summarised as follow:

pAGB Stars. A tight correlation between the stellar surface brightness and the flux of the H β recombination line throughout the vast majority of our sample galaxies points to a diffuse and old stellar source as the main contributor of ionising photons in early-type galaxies. Based on simple ionisation-balance arguments we have shown that since the initial suggestion of Binette et al. (1994) pAGB stars remain the favourite candidate for powering the ionised-gas emission of early-type galaxies, which urges further investigations into the present discrepancy between observations and models as regards their total numbers.

AGN. The presence of a radio or X-ray core suggests the additional role of AGN photoionisation in approximately 30% of the galaxies in our sample, although the radial profile of the H β recombination line shows that a central source can be responsible for the observed emission at best only within a few hundred parsecs from the centre, corresponding to the innermost $2'' - 3''$.

Shocks. Fast shocks are unlikely to be an important source of ionisation for the extended nebular emission observed in early-type galaxies, even where spiral or integral-sign gas structures are accompanied by a similar [O III]/H β feature. Indeed, the shock velocities required to power the nebular emission can hardly be attained in the potential of our sample galaxies, in particular given the relatively relaxed gas kinematics that is observed in them.

OB-stars. Extremely low values of the [O III]/H β ratio leave no doubt that OB-stars are powering most of the nebular emission observed in 6% of the SAURON sample galaxies (3/48), whereas the presence of regular dust morphologies, relaxed gas kinematics, young stellar populations, molecular gas, PAH features and strong FIR fluxes further support the case for on-going star formation in up to 10% of the sample (5/48). In these objects star formation appears confined mostly to circumnuclear regions, which in two cases is confirmed by [N I]/H β diagnostic diagrams that highlight the role of other sources of ionisation outside of the ring regions, for instance of a central AGN towards the centre. Yet, star formation may have proceeded also outside these circumnuclear regions, in particular in the least massive galaxies like NGC 3032 where younger stellar populations are found throughout the entire SAURON field of view.

Post-starburst pAGB Stars. For another 10% of the SAURON sample, consisting too of low-mass objects, the intense and highly-ionised emission relates also to a recent and spatially extended star-formation episode, although the principal ionising sources are no longer OB-stars but the pAGB population associated to the younger stellar subcomponent.

Interaction with the Hot Phase. At the opposite end of the mass spectrum, we find that in the brightest and slowly- or non-rotating early-type galaxies the ability to retain massive halo of hot,

⁴ See also <http://purl.org/atlas3d>

X-ray emitting gas corresponds to a distinct low-ionisation character of the emission-line regions and to a remarkable spatial coincidence between optical and X-ray emitting features. These findings testify to an interaction between the hot and warm phases of the ISM that provides an additional excitation mechanism besides photoionisation by old stellar sources.

The prominent role of old stellar sources over other ionising mechanisms in powering the nebular emission of early-type galaxies, taken together with the extended character that ionised gas always displays in our sample, motivated us to explore the nature of the ionised-gas emission that is observed in early-type galaxies at larger distances through large physical apertures, as in the case of the SDSS spectroscopic data. We have exploited the integral-field nature of our data to integrate the SAURON spectra of our sample galaxies over increasingly wider circular apertures as to mimic the spectra of increasingly distant objects observed through the fixed 3''-wide SDSS aperture. We measured the values for the [O III] equivalent width and the [O III]/H β ratio for the total emission in such apertures and compared our results with the emission-line measurements for the morphologically-selected sample of early-type galaxies of Schawinski et al. (2007). Even accounting for the incomplete character of the SAURON sample, our data suggest that in very few, if any, of the SDSS galaxies which display only modest values for the equivalent width of the [O III] line (less than $\sim 2.4\text{\AA}$) and LINER-like values for the [O III]/H β ratio, the nebular emission is truly powered by AGN activity. Only the most intense, and rarer, manifestations of LINER nuclear activity can be detected against both the stellar background encompassed by the SDSS aperture and the diffuse emission of early-type galaxies. The latter, when detected through SDSS spectra, is usually powered by pAGB stars associated either to old stellar populations or to a recent star-formation episode.

ACKNOWLEDGEMENTS

MS is grateful to Mark Allen, Aaron Barth, Igor Chilingarian, Alison Crocker, Brent Groves, Guenevieve Graves, Luis Ho, Sadegh Khochfar, John Magorrian, Gary Mamon, Ralph Napietowski, Carlo Nipoti, Martin Hardcastle and Philipp Podsiadlowski for many fruitful discussions. We are also grateful to Alexandre Vazdekis and Mark Allen for providing us with their latest models prior to publication, and to the anonymous referee for his/her useful comments. MS and MC also acknowledge support from their respective STFC Advanced Fellowships.

REFERENCES

- Allen M. G., Groves B. A., Dopita M. A., Sutherland R. S., Kewley L. J., 2008, *ApJS*, 178, 20
 Bacon R., et al., 2001, *MNRAS*, 326, 23
 Baldwin J. A., Phillips M. M., Terlevich R., 1981, *PASP*, 93, 5
 Becker R. H., White R. L., Helfand D. J., 1995, *ApJ*, 450, 559
 Binette L., Magris C. G., Stasińska G., Bruzual A. G., 1994, *A&A*, 292, 13
 Böhringer H., et al., 2000, *ApJS*, 129, 435
 Brown, T. M., Smith, E., Ferguson, H. C., Sweigart, A. V., Kimble, R. A., & Bowers, C. W. 2008, *ApJ*, 682, 319
 Buyle P., Michielsen D., De Rijcke S., Pisano D. J., Dejonghe H., Freeman K., 2006, *ApJ*, 649, 163
 Caplan J., Deharveng L., 1986, *A&A*, 155, 297
 Cappellari M., Renzini A., Greggio L., di Serego Alighieri S., Buson L. M., Burstein D., Bertola F., 1999, *ApJ*, 519, 117
 Cappellari M., Copin Y., 2003, *MNRAS*, 342, 345
 Cappellari M., et al., 2006, *MNRAS*, 366, 1126
 Cappellari M., et al., 2007, *MNRAS*, 379, 418
 Caldwell N., 1984, *PASP*, 96, 287
 Combes F., Young L. M., Bureau M., 2007, *MNRAS*, 377, 1795
 Condon J. J., 1992, *ARA&A*, 30, 575
 Dehnen W., 1993, *MNRAS*, 265, 250
 de Jong T., Norgaard-Nielsen H. U., Jorgensen H. E., Hansen L., 1990, *A&A*, 232, 317
 de Vaucouleurs G., 1948, *AnAp*, 11, 247
 de Zeeuw P. T., et al., 2002, *MNRAS*, 329, 513
 Donahue M., Voit G. M., 1991, *ApJ*, 381, 361
 Donahue M., Voit G. M., 1993, *ApJ*, 414, L17
 Dopita M. A., Sutherland R. S., 1995, *ApJ*, 455, 468
 Dopita M. A., Sutherland R. S., 1996, *ApJS*, 102, 161
 Dopita M. A., Koratkar A. P., Allen M. G., Tsvetanov Z. I., Ford H. C., Bicknell G. V., Sutherland R. S., 1997, *ApJ*, 490, 202
 Dopita M. A., Kewley L. J., Heisler C. A., Sutherland R. S., 2000, *ApJ*, 542, 224
 Dopita M. A., Groves B. A., Sutherland R. S., Binette L., Cecil G., 2002, *ApJ*, 572, 753
 Dressler A., Gunn J. E., 1983, *ApJ*, 270, 7
 Emsellem E., Goudfrooij P., Ferruit P., 2003, *MNRAS*, 345, 1297
 Emsellem E., et al., 2004, *MNRAS*, 352, 721
 Emsellem E., et al., 2007, *MNRAS*, 379, 401
 Trinchieri G., Fabbiano G., Canizares C. R., 1986, *ApJ*, 310, 637
 Fabbiano G., Kim D.-W., Trinchieri G., 1992, *ApJS*, 80, 531
 Fabian A. C., 1994, *ARA&A*, 32, 277
 Falcón-Barroso J., et al., 2006, *MNRAS*, 369, 529
 Ferland G. J., Netzer H., 1983, *ApJ*, 264, 105
 Ferland G. J., Korista K. T., Verner D. A., Ferguson J. W., Kingdon J. B., Verner E. M., 1998, *PASP*, 110, 761
 Ferland G. J., Fabian A. C., Hatch N. A., Johnstone R. M., Porter R. L., van Hoof P. A. M., Williams R. J. R., 2009, *MNRAS*, 392, 1475
 Filho M. E., Fraternali F., Markoff S., Nagar N. M., Barthel P. D., Ho L. C., Yuan F., 2004, *A&A*, 418, 429
 Giroletti M., Taylor G. B., Giovannini G., 2005, *ApJ*, 622, 178
 Goudfrooij P., Hansen L., Jorgensen H. E., Norgaard-Nielsen H. U., 1994, *A&AS*, 105, 341
 Goudfrooij P., 1999, *ASPC*, 163, 55
 Graves G. J., Faber S. M., Schiavon R. P., Yan R., 2007, *ApJ*, 671, 243
 Greggio, L., Renzini, A., 1990, *ApJ*, 364, 35
 Groves B. A., Dopita M. A., Sutherland R. S., 2004, *ApJS*, 153, 75
 Irwin J. A., Athey A. E., Bregman J. N., 2003, *ApJ*, 587, 356
 Jaffe W., 1983, *MNRAS*, 202, 995
 Jeong H., Bureau M., Yi S. K., Krajnović D., Davies R. L., 2007, *MNRAS*, 376, 1021
 Jeong H., et al., 2009, *MNRAS*, 398, 2028
 Hatch N. A., Crawford C. S., Johnstone R. M., Fabian A. C., 2006, *MNRAS*, 367, 433
 Heckman T. M., Baum S. A., van Breugel W. J. M., McCarthy P., 1989, *ApJ*, 338, 48
 Heckman T. M., 1980, *A&A*, 87, 152
 Hernquist L., 1990, *ApJ*, 356, 359
 Ho L. C., Shields J. C., Filippenko A. V., 1993, *ApJ*, 410, 567
 Ho L. C., Filippenko A. V., Sargent W. L. W., 1997, *ApJS*, 112, 315

- Ho L. C., 2008, *ARA&A*, 46, 475
- Hu E. M., Cowie L. L., Wang Z., 1985, *ApJS*, 59, 447
- Kaneda H., Onaka T., Sakon I., 2005, *ApJ*, 632, L83
- Kauffmann, G., et al. 2003, *MNRAS*, 346, 1055
- Kauffmann G., Heckman T. M., 2009, *MNRAS*, 397, 135
- Kawata D., Cen R., Ho L. C., 2007, *ApJ*, 669, 232
- Kaviraj S., Kirkby L. A., Silk J., Sarzi M., 2007, *MNRAS*, 382, 960
- Kennicutt R., 1983, *A&A*, 120, 219
- Kewley L. J., Dopita M. A., Sutherland R. S., Heisler C. A., Trevena J., 2001, *ApJ*, 556, 121
- Kewley L. J., Groves B., Kauffmann G., Heckman T., 2006, *MNRAS*, 372, 961
- Kim D.-W., 1989, *ApJ*, 346, 653
- Kim D.-W., Fabbiano G., 2004, *ApJ*, 611, 846
- Kuntschner H., et al., 2006, *MNRAS*, 369, 497
- Laing R. A., Bridle A. H., 1987, *MNRAS*, 228, 557
- Leitherer C., et al., 1999, *ApJS*, 123, 3
- Liebert J., Saffer R. A., Green E. M., 1994, *AJ*, 107, 1408
- Macchetto F., Pastoriza M., Caon N., Sparks W. B., Giavalisco M., Bender R., Capaccioli M., 1996, *A&AS*, 120, 463
- Mathews W. G., Brighenti F., 2003, *ARA&A*, 41, 191
- Mazzuca L. M., Sarzi M., Knapen J. H., Veilleux S., Swaters R., 2006, *ApJ*, 649, L79
- Morganti R., et al., 2006, *MNRAS*, 371, 157
- O'Sullivan E., Forbes D. A., Ponman T. J., 2001, *MNRAS*, 328, 461
- Owen, F. N., Hardee, P. E., & Cornwell, T. J. 1989, *ApJ*, 340, 698
- Pellegrini S., 2005, *MNRAS*, 364, 169
- Phillips M. M., Jenkins C. R., Dopita M. A., Sadler E. M., Binette L., 1986, *AJ*, 91, 1062
- Rappaport S., Chiang E., Kallman T., Malina R., 1994, *ApJ*, 431, 237
- Renzini A., Greggio L., di Serego-Alighieri S., Cappellari M., Burstein D., Bertola F., 1995, *Nature*, 378, 3
- Sabra B. M., Shields J. C., Filippenko A. V., 2000, *ApJ*, 545, 157
- Sabra B. M., Shields J. C., Ho L. C., Barth A. J., Filippenko A. V., 2003, *ApJ*, 584, 164
- Sánchez-Blázquez P., et al., 2006, *MNRAS*, 371, 703
- Sarzi M., Rix H.-W., Shields J. C., Ho L. C., Barth A. J., Rudnick G., Filippenko A. V., Sargent W. L. W., 2005, *ApJ*, 628, 169
- Sarzi M., et al., 2006, *MNRAS*, 366, 1151
- Schawinski, K., Thomas, D., Sarzi, M., Maraston, C., Kaviraj, S., Joo, S.-J., Yi, S. K., & Silk, J. 2007, *MNRAS*, 382, 1415
- Shapiro K., L., et al., 2009, submitted
- Shields J. C., 1991, *AJ*, 102, 1314
- Shields J. C., Kennicutt R. C., Jr., 1995, *ApJ*, 454, 807
- Shull J. M., McKee C. F., 1979, *ApJ*, 227, 131
- Sparks W. B., Macchetto F., Golombek D., 1989, *ApJ*, 345, 153
- Sparks W. B., Donahue M., Jordán A., Ferrarese L., Côté P., 2004, *ApJ*, 607, 294
- Stasińska G., Leitherer C., 1996, *ApJS*, 107, 661
- Stasińska, G., Vale Asari, N., Cid Fernandes, R., Gomes, J. M., Schlickmann, M., Mateus, A., Schoenell, W., & Sodré, L., Jr. 2008, *MNRAS*, 391, L29
- Taniguchi Y., Shioya Y., Murayama T., 2000, *AJ*, 120, 1265
- Trinchieri G., Goudfrooij P., 2002, *A&A*, 386, 472
- Vazdekis A., et al., 2007, *IAUS*, 241, 133
- Vazdekis A., et al., 2009, submitted
- Veilleux S., Osterbrock D. E., 1987, *ApJS*, 63, 295
- Voit G. M., Donahue M., 1990, *ApJ*, 360, L15
- Yi S., Lee Y.-W., Woo J.-H., Park J.-H., Demarque P., Oemler A. J., 1999, *ApJ*, 513, 128
- Young A. J., Wilson A. S., Mundell C. G., 2002, *ApJ*, 579, 560
- Young L. M., Bureau M., Cappellari M., 2007, *ApJ*, submitted
- Wrobel J. M., 1991, *AJ*, 101, 127